M 2023

U.PORTO
FEUP FACULDADE DE ENGENHARIA
UNIVERSIDADE DO PORTO

EMERGING MATERIALS FOR THIN-FILM SOLAR CELLS

MARIA CATARINA DA SILVA CORTEZ
MASTER THESIS IN CHEMICAL ENGINEERING
PRESENTED TO THE FACULTY OF ENGINEERING
OF THE UNIVERSITY OF PORTO

Master in Chemical Engineering

Emerging materials for thin-film solar cells

Master Dissertation

of

Maria Catarina da Silva Cortez

Developed within the course of Dissertation

held at

INL - International Iberian Nanotechnology Laboratory

Supervisor at FEUP: **Prof. Adélio Mendes**

Coordinator at INL - International Iberian Nanotechnology Laboratory: **Dr. Sascha Sadewasser**

March 2023

Acknowledgment

Firstly, in my gratitude is an expression of thanks to my parents, Mário and Manuela, for all their support and sacrifices throughout the years. Thank you so much for always standing behind every choice I made and pushing towards accomplishing all that was once just a dream!

My gratitude extends wholeheartedly to Diego Garzón, whose wise counsel and knowledge have been of great value. I am deeply appreciative of your support each time I ventured into uncharted territories during my work endeavors. I will always cherish all the karaoke sessions done in the lab.

A deep sense of gratitude goes out to Prof. Adélio Mendes, who made this project possible and supported me throughout this journey. I am deeply grateful for always being there whenever I needed, as well as all the valuable teachings and knowledge sharing.

To Dr. Sascha Sadewasser, I want to express my gratitude, not only for proposing this project but also for all the invested time and patience in teaching me. His contribution to this project has been immense, and I'm grateful for his unwavering support throughout.

I also want to leave a special thank you to all LaNaSC group for making me feel so welcome. Thank you for all the help and guidance.

I express my sincere gratitude to those who have accompanied me throughout this path, including all dearest friends and beloved members of family.

Abstract

Chalcogenide perovskites are an emerging type of material with possible applications in photovoltaic technology that are considered to be robust, have earth-abundant materials, and represent a nontoxic option for energy conversion technologies. Therefore, an attempt to make a chalcogenide perovskite of magnesium tin selenide ($MgSnSe_3$) was carried out via chemical bath deposition (CBD). CBD is a method that is low-cost and easily reproducible.

The chalcogenide perovskite was deposited on fluorine-doped tin oxide glass (FTO). The deposition of the binary compounds suffered an optimization process. It was possible to conclude that an increase in temperature made the thin films more homogenous. Since the agitation of the baths in CBD can improve the quality of the deposition, the CBD using ultrasound was studied. However, the films did not improve.

The attempt to make a selenium-based chalcogenide perovskite was made in two steps, MgSe was deposited on SnSe or SnSe was deposited on MgSe, and afterward, a heat treatment, to synthesize the perovskite and try to increase its crystallinity. This co-deposition made the thin films more homogenous.

The selenium-based chalcogenide perovskite could not be synthesized. The formation of oxide-based perovskites is more stable than selenide-based perovskites. On another note, the construction of a selenide-based perovskite is less stable than the formation of a sulphide-based perovskite. Therefore, it was attempted the manufacture an oxide-based perovskite ($MgSnO_3$) and a sulphide-based perovskite ($MgSnS_3$). It wasn't possible to conclude the formation of $MgSnO_3$ or $MgSnS_3$.

Keywords (theme): Chalcogenide perovskite, Chemical Bath Deposition, Photovoltaic technology

Resumo

As perovskitas calcogénicas são um tipo emergente de material com possíveis aplicações na tecnologia fotovoltaica que são consideradas robustas, têm materiais abundantes na Terra, e representam uma opção não tóxica para as tecnologias de conversão de energia. Por conseguinte, foi feita uma tentativa de fazer uma perovskita calcogénica de seleneto de estanho de magnésio ($MgSnSe_3$) através da deposição em banho químico (CBD). A CBD é um método de baixo custo e facilmente reprodutível.

A perovskita calcogénica foi depositada em vidro de óxido de estanho dopado com flúor (FTO). A deposição dos compostos binários sofreu um processo de otimização. Foi possível concluir que o aumento da temperatura tornou os filmes de película fina mais homogéneos. Uma vez que a agitação dos banhos em CBD pode melhorar a qualidade da deposição, foi estudada a CBD utilizando ultrassons. No entanto, os filmes de película fina não melhoraram.

A tentativa de fazer uma perovskita calcogénica à base de selénio foi feita em duas etapas, MgSe foi depositado em SnSe ou SnSe foi depositado em MgSe, e depois, um tratamento térmico, para sintetizar a perovskita e tentar aumentar a sua cristalinidade. Esta co-deposição tornou os filmes de película fina mais homogéneos.

A perovskita calcogénica à base de selénio não pôde ser sintetizada. A formação de perovskitas à base de óxido é mais estável do que a formação de perovskitas à base de selenetos. Por outro lado, a construção de uma perovskita à base de selénio é menos estável do que a formação de uma perovskita à base de sulfureto. Por conseguinte, tentou-se fabricar uma perovskita à base de óxido ($MgSnO_3$) e uma perovskita à base de sulfureto ($MgSnS_3$). Não foi possível concluir a formação do $MgSnO_3$ ou do $MgSnS_3$.

Palavras-chave (tema): Perovskita calcogénica, Deposição em banho químico, Tecnologia Fotovoltaica

Declaration

I hereby declare, under word of honor, that this work is original and that all non-original contributions are indicated, and due reference is given to the author and source.

Porto, 13 de Março de 2023

Maria Catarina da Silva Cortez

Index

List of Figures

List of Tables

Notation and Glossary

ΔX	relative change in cation-anion electronegativity difference relative to oxygen	
E_g	band gap energy	J
h	Plank's constant	J·s
K_{sp}	solubility product constant	
t	Goldschmidt tolerance factor	
t^*	modified Goldschmidt tolerance factor	
r_A	ionic radii for the A-site of the perovskite structure	m
r_B	ionic radii for the B-site of the perovskite structure	m
r_X	ionic radii for the X-site of the perovskite structure	m
v	photon's frequency	s^{-1}

Greek Letters

α	energy-dependent absorption coefficient	cm^{-1}
γ	factor dependent on the electronic transition	

List of Acronyms

CBD	Chemical bath deposition
CIGS	Copper indium gallium selenide
DIW	Deionized water
EDX	Energy-dispersive X-ray spectroscopy
ETA	Ethanolamine
ETL	Electron transport layer
FTO	Fluorine-doped tin oxide glass
HTL	Hole transport layer
INL	International Iberian Nanotechnology Laboratory
LaNaSC	Laboratory for Nanostructured Solar Cells
PV	Photovoltaic
SEM	Scanning electron microscopy
SILAR	Successive Ionic Layer Adsorption and Reaction
SLG	Soda–lime–silica glass
TCO	Transport conductive oxide
TEA	Triethanolamine
UV-Vis	Ultraviolet-visible spectrophotometry
XRD	X-ray diffraction

1 Introduction

1.1 Framing and presentation of the work

Excess carbon dioxide emissions to the atmosphere from fossil fuels have resulted in high greenhouse gas concentrations, rising sea levels, rising ocean temperatures, and acidification of the oceans. As a result, having access to energy in a sustainable manner has become essential.

That goal is achievable with renewable energy sources such as photovoltaic (PV) panels. The Sun is an infinite and free resource, and solar cells are known to have low environment impact, neither chemically nor through noise. [1]

PV technology can generate electrical energy at a lower cost while also being environmentally friendly. Therefore, solar cells made from readily available materials (semiconductors) are vital for widespread photovoltaic electricity generation deployment. [2] Solar cells do not detain a specific classification, but normally they are categorized by different types of technology. First Generation PVs correspond to silicon-based single crystalline and polycrystalline solar cells (which are currently the most commercialized). Second-Generation solar cells are based on thin-film technology; there are amorphous silicon, CIGS (Copper Indium Gallium Selenide), CdTe (Cadmium Telluride) and GaAs (Gallium Arsenide) solar cells. The copper zinc sulfide solar cells, organic solar cells, quantum dot solar cells, dye-sensitized solar cells, and perovskite solar cells comprehend Third-Generation technology for solar cells. [3]

For PV applications, the band gap is an important parameter that determines the possible functionality of a specific semiconductor (material that can conduct electricity). This value corresponds to the minimum amount of energy needed to excite an electron from the valence band in a semiconductor to a higher energy state. Only photons with energies greater than or equal to the band gap of a material can be absorbed. [4]

A solar cell generates power by converting photons in hole-electron pairs, which generates current. When large band gaps are used, there is a higher maximum voltage that can be achieved, however, that results in reduced sunlight absorption and reduced current. [4] In the case of perovskite solar cells, the perovskite presents a low band gap which promotes the absorption of high-energy photons in the visible solar spectrum's blue and green regions. [3]

Perovskite solar cells are based in a perovskite absorber material, which displays a basic chemical representation exemplified by the formula ABX_3, where A and B represent 2+ and 4+ cations, respectively, and X represents an anion with charge 2-. The development of a

perovskite structure is dependent on ion charge neutrality, the stability of BX_6 octahedra, and the ionic radii of the constituent ions, A, B, and X.[5]

The perovskite solar cells began with perovskite oxides but were not further studied as PV materials because they required high temperatures to form and had a limited application due to their wide band gap, which led them to harvest less than 8% of the solar spectrum. To overcome this limitation, it has been proposed to replace the oxide perovskite with an inorganic halide anion. [6]

Halide perovskite layers could be formed at low temperatures (from 80 to 150 °C) using simple solution-based approaches. However, these perovskite solar cells face long-term stability challenges like degradation due to heat, pressure, or even moisture. [7] Such challenges can be addressed through encapsulation, but the desired solution lies in modifying the intrinsic properties of the perovskite materials. [6]

Unlike halide perovskites, chalcogenide compounds have a high level of environmental stability. [6] Chalcogenide perovskites have the basic chemical representation of perovskites; however, X represents a chalcogen anion such as S, Se, or Te. [8]

The crystal structure influences optoelectronic properties such as the band-gap suitable for solar cells and efficient light absorption. As a result, a thorough understanding of stable phase formation in perovskites is required. [8]

The Goldschmidt tolerance factor, t, is a general indicator of the thermodynamic stability of the 3D oxide perovskite structure. Unfortunately, this factor fails to correlate the reported stable phases and the tolerance factor for chalcogenide perovskites, so Jess et al. 2022 proposed the modified Goldschmidt tolerance factor, t^*. This factor predicts a perovskite structure when it is greater than 0.83 for oxide perovskites, greater than 0.94 for sulphide compounds, and greater than 1.01 for selenide compounds. [8]

A thin film is represented by a single layer or a combination of layers of one or more materials that are deposited on a surface and can be used to modify the properties of the support substrate or to develop a device. [9] For years, chalcogenide thin films have captured the attention of researchers due to factors such as earth abundance, environmental friendliness, and excellent structural, electrical, and optical properties. [10]

Thin films on substrates can be grown using a variety of physical and chemical deposition techniques. Numerous deposition processes are available including spray pyrolysis, electrodeposition method, chemical vapour deposition, spin coating, successive ionic layer adsorption and reaction (SILAR), physical vapour deposition, sputtering, and chemical bath deposition. [11]

Spray pyrolysis is a method of depositing a thin film on a heated surface by spraying a solution, where the constituents react to form a chemical compound. [10] Another chemical technique is electrodeposition and is the controlled deposition of a material on conducting surfaces using an electric current from an ionic species-containing solution. Even so, it cannot be used for large-scale production. [11]

Chemical vapour deposition is a vacuum deposition method that is used to create high-quality, high-performance solid materials. Moreover, high temperatures are used in this process. [11]

Spin coating is a technique that uses centrifugal force to spread uniform thin films on flat substrates. However, caution is advised since high-speed spinning becomes extremely difficult as the size of the substrate increases. [11]

SILAR can be utilized to deposit ultra-thin coatings on desired substrates and can be performed at ambient pressure. In this process, a simple dip coating unit can be used, and the cost associated with this procedure is considered low. [9]

Physical vapor deposition is a technique that is better suited for thick films (in the range of one thousand nanometers) and requires a high vacuum pressure. For the other physical technique, sputtering, films are produced with high adhesion and uniform morphology, but it is a very expensive process with a low deposition rate. [11]

Chemical Bath Deposition (CBD) has a long history of producing semiconductor layers for photovoltaic applications. [12] This approach is widely used for thin film deposition because it is low-cost, convenient for broad area deposition, and provides the ability to tailor thin film properties by changing and manipulating the deposition parameters. The bath is assumed to be thermodynamically unstable and supersaturated, resulting in precipitation. [9] Depending on the deposition time, this process can produce films with a thickness of around 500 nm. [13] Nevertheless, this process produces a waste of solution. [11]

Chalcogenide perovskites have promising optoelectronic properties such as strong solar spectrum absorption, easy charge transport, and high thermodynamic and atmospheric stability. Their synthesis, however, remains a significant challenge, with only a few sulphide compositions reported in the literature. [7] Except for mixed sulphide and selenide compositions, selenide perovskites have yet to be successfully synthesized. [14] These materials are typically synthesized using solid-state reactions and the processes can use temperature of around 1000 °C. [7]

Various techniques will be used to characterize the samples, including scanning electron microscopy (SEM), energy-dispersive X-ray spectroscopy (EDX), Raman, UV-Vis transmittance, and x-ray diffraction (XRD). By scanning a focused electron beam across the surface and

detecting secondary or backscattered electron signals, SEM produces high-resolution images of the sample. The EDX analyser provides elemental identification as well as quantitative compositional data. The Raman spectrum is a distinct chemical signature for a particular molecule or material. Using the Tauc method, integrating spheres can be used to measure transmittance and determine the bandgap of a thin film. [15] When planes in the crystal lattice are exposed to an X-ray beam, XRD measures the scattering of X-rays and can determine the crystal structure of a material.

Due to the difficulty of synthesizing a chalcogenide perovskite, two different binary components will be deposited by CBD. Magnesium tin selenide ($MgSnSe_3$) was chosen as the compound to synthesize since its earth-abundant and has a modified Goldschmidt factor of 1.23. This anion was chosen to begin the project due to LaNaSC group's prior knowledge of creating selenide materials. Furthermore, both binary salts (MgSe and SnSe) are already reportedly manufactured by this method [16] [17] A subsequent annealing process in a tube furnace will be performed to improve the crystallinity of the chalcogenide perovskite as reported by Shahzad et al. 2020.

1.2 Presentation of the company

INL (International Iberian Nanotechnology Laboratory) in Braga houses the Laboratory for Nanostructured Solar Cells (LaNaSC). The LaNaSC mission is to develop nano- and micro-structures for photovoltaic energy conversion applications. Hence, it has been involved in several solar initiatives, including work on CIGS Solar Cells. As the group is currently focusing on the development of new photovoltaic materials, the investigation of stable, Pb-free perovskites is a logical next step in PV research.

1.3 Contribution of the author to the work

All depositions were conducted by me, as well as the designs of all the processes for it. I did all the characterizations for Raman, SEM, EDX and UV-Vis Transmittance, as well as the XRD analysis.

Due to my experience in Chemical Laboratories, I was able to bring safety measures to the group, which primarily consists of Physical Engineers and Physicists, such as the adoption of Safety Data Sheets near the chemicals and better reagent organization.

I also had the opportunity to bring good laboratory practices that I had learned and developed throughout my degree and had the opportunity to assemble a high precision balance while working on my thesis.

1.4 Organization of the dissertation

This dissertation will be divided into six sections. There will be an introduction that will discuss the areas of this project. Context and State of the Art follow, which describe the areas of this work and what has been done so far. Following that, the process is described in Materials and Methods, and the results are presented and explored in Results and Discussion. The main findings of this dissertation are then presented in the Conclusion. Finally, the Assessment of Work Done comments on whether the objectives were met and what should be done in the future.

2 Context and State of the art

The accelerated growth of human population has resulted in a rise in worldwide energy consumption. Most of the energy consumed is still generated from non-renewable fossil fuels, which contributes to increasingly high levels of greenhouse gas emissions. Also, fossil fuels do not renew themselves in a timely enough manner to be considered renewable. [3]

Therefore, it is important to search for new alternative sources of renewable energy. Solar energy could become a viable option for a sustainable production of energy. But several photovoltaic cells are reliant on materials with a limited concentration on the crust of the Earth, which impacts their sustainability. As such, research on emerging materials for solar cells has been receiving more attention. [3]

2.1 PV technologies

Silicon solar cells are the most widely available on the market due to their high photo-conversion efficiency, stability, low cost because all the research done to date, and abundance of silicon on Earth. [3] However, silicon presents an indirect bandgap of 1.12 eV, which limits the amount of energy harvestable from the solar spectrum. [6]

Thin-film technology is the foundation of Second-Generation photovoltaics; it is lightweight and flexible, but there are toxicity and environmental concerns, as well as concerns about stability and durability. [3] As a PV technology, the materials for this generation are less developed and are typically deposited by vacuum-assisted or chemical vapour deposition. Despite their low cost, their efficiencies are lower than Si-based PV, but they can be made much thinner and lighter than First-Generation solar cells. [6]

The Third-Generation emerging solar cells are a low cost, and fast-growing technology with comparatively easy manufacturing, they also have great potential for further improvement, and they are lightweight and flexible. On the other hand, it is a young technology with low stability and durability, and some compounds may cause toxicity and environmental problems. Perovskite-Silicon tandem solar cells, Perovskite solar cells, Organic solar cells, Dye-sensitized solar cells, Copper Zinc Sulphide solar cells, and Quantum Dot solar cells are all included in this category. [3]

This work focuses on chalcogenide-perovskite solar cells, which are classified as Third-Generation Solar Cells. The foundation for perovskite solar cells is solid-state sensitized solar cells based on dye-sensitized solar cells. [19]

2.2 Perovskite solar cells working principle

The photovoltaic effect causes voltage to be generated in a solar cell. An external incident particle, such as a photon, can excite the charge carrier electron to the conduction band, leaving a hole behind in the valence band. [20]

Figure 2-1 shows the standard structure of a perovskite solar cell, which is based on the stack of five layers: the counter electrode, the hole transport layer (HTL), the perovskite layer, the electron transport layer (ETL), and the transparent conductive oxide (TCO) placed on a glass substrate. [3] Between the layers, the core layer corresponds to the perovskite layer, which absorbs the light and produce electron-hole pairs. Due to this charge separation in the pn junction, a voltage is generated, which is the principle of the photovoltaic effect.

The HTL and ETL layers can transport holes and electrons, respectively. The HTL can also avoid metal-perovskite interface degradation. Furthermore, the ETL inhibits hole backflow and hence assures charge separation to avoid unwanted charge recombination. [3]

The counter electrode and the TCO capture holes and electrons from the HTL and ETL, respectively. In addition, they allow the electron and hole recombination to produce current outside the closed circuit. Finally, the glass substrate serves as a foundation for the solar cell. [3]

According to the literature, TCO is typically fluorine-doped tin oxide glass (FTO) or indium tin oxide glass. In addition, gold is the most used counter electrode, but platinum is also used. The ETL is typically composed of titanium oxide. [3]

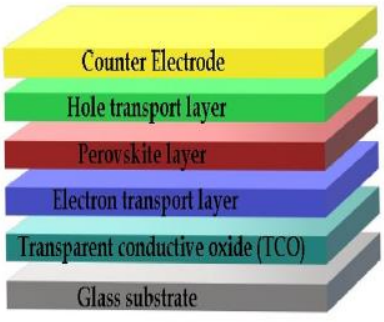

Figure 2-1 - The fundamental structure of a perovskite solar cell [3]

Currently, the challenge consists in commercializing perovskite solar cells, mainly improving their efficiency and stability. The known methods require high temperatures and vacuum conditions, which creates difficulties when upscaling the processes. [3]

In the search for efficient and sustainable solar cell materials, it is critical to concentrate on elements that are abundant on Earth and are environmentally safe. Among other things, ideal materials should have high light absorption per unit thickness, excellent charge carrier

transport properties, and be thermodynamically stable. [4] When assessing the potential of a possible PV material, band gap stands out as a critical factor.

2.3 Chalcogenide Perovskites

Chalcogenide Perovskite Solar Cells are a promising type of solar cell because they are low-cost, environmentally friendly (when compared to the Pb-based halide perovskites), and long-lasting (high structure stability), all of which are goals that industries are currently pursuing. [14]

Since optoelectronic properties are highly dependent on crystal structure, understanding the stable phase formation in these ABX_3 compounds is essential. The Goldschmidt tolerance factor (t) is frequently used to predict stable phase formation of oxide perovskites, however this tolerance factor fails to predict the resulting stable phase of some compounds, since it doesn't show a correlation between the tolerance factor and the reported stable phase. [8]

To close that gap, Jess et al. 2022 proposed a modified Goldschmidt tolerance factor, t^*. Figure 2-2 shows the modified tolerance factor for some possible chalcogenide perovskites. This factor accommodates for the variations in the bond lengths of constituent atoms in the ABX_3 structure due to electronegativity discrepancies between oxide and chalcogenide perovskites. The BX_6 octahedra corresponds to the connection between X, that forms the corner, and the B ion, that forms the center. It is also important to mention that the octahedral factor corresponds to the ratio between the ionic radius of the B cation and the ionic radius of the X anion. [8]

The modified Goldschmidt tolerance factor, t^* uses the ionic radii for the A-site (r_A), B-site (r_B) and chalcogen atoms in the crystal lattice (r_X). This modified factor differs from the original by utilizing the relative change in cation-anion electronegativity difference ΔX relative to oxygen, as can be defined by equation 2.1,

$$t^* = \frac{\frac{\Delta X_{(A-X)}}{\Delta X_{(A-O)}}(r_A + r_X)}{\sqrt{2}\frac{\Delta X_{(B-X)}}{\Delta X_{(B-O)}}(r_B + r_X)} \tag{2.1}$$

To create efficient direct-bandgap semiconductors for optoelectronics, both ideal and distorted perovskite structures require corner-sharing octahedra. This results in high absorption in the relevant energy range, isotropy, and high electron mobility. This is due to the high symmetry and electron configuration on the B-site cation, as well as B-X antibonding bond, which results in dispersive electronic bands. Due to a decrease in octahedral and tolerance factors, selenide perovskites are less thermodynamically stable than sulphide perovskites. [8]

Lowering the electronegativity difference along the B-X bond can result in a smaller band gap, which is beneficial for optoelectronic applications in the visible and infrared spectrums. Because of the lower electronegativity difference in the B-X bond, chalcogenide perovskites are promising materials for solar cells and other optoelectronic applications. A high electronegativity difference along the B-X bond, on the other hand, often results in a wider band gap insulator in oxide perovskites. [21]

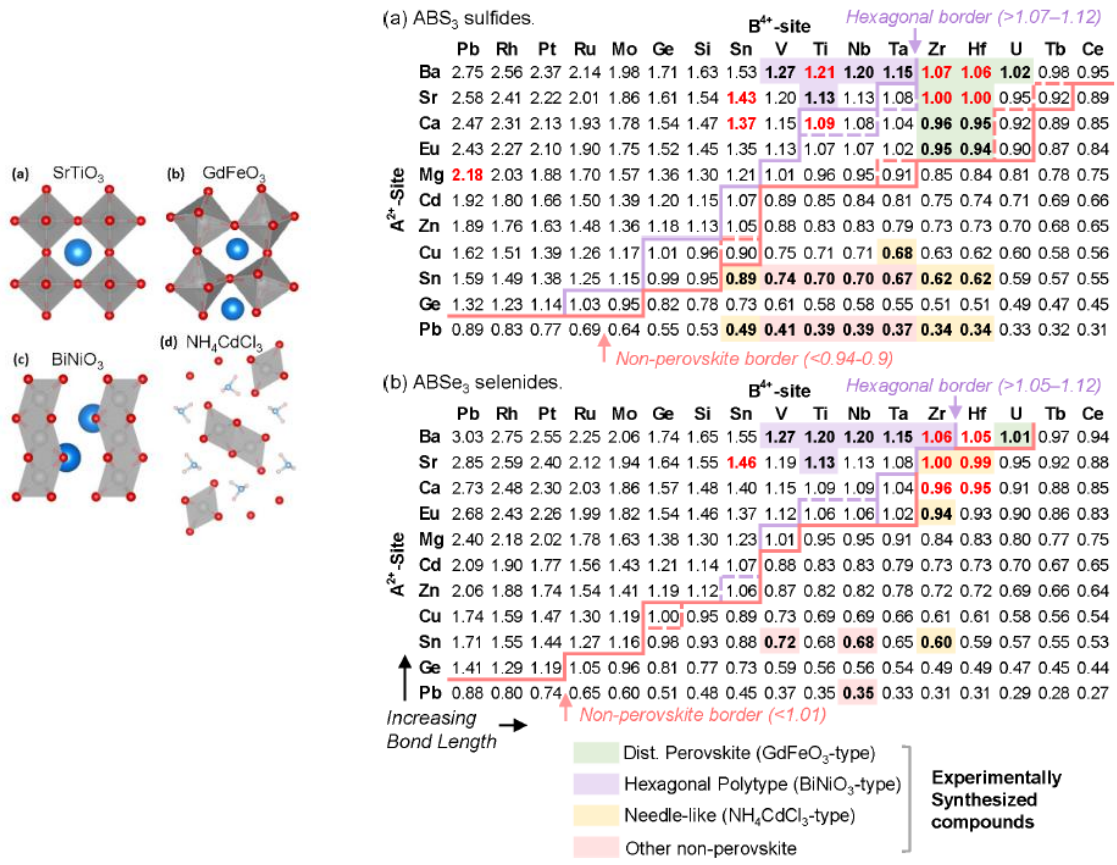

Figure 2-2 - Modified Goldschmidt tolerance factor for ABS_3 and $ABSe_3$ compounds, with the common structural polytypes for ABX_3. In the perovskite structures, the A-site cation can be seen as blue, the B-site cation as grey and the anion corresponds to the red, for different materials. [8]

The synthesis of ABX_3 chalcogenide perovskites in a variety of stable phases has been reported numerous times over the last 60 years. [22]–[25] However, there is insufficient evidence of any selenide perovskites synthesized except for those that contain uranium. [7] The most well-known and discussed compound, however, is the $BaZrS_3$ compound. Despite being a promising researched perovskite with band gap reports of around 1.75 eV, it is prepared at high temperatures of around 1000 °C. [21]

The materials studied for this project were based on the stability of the perovskites calculated through the modified Goldschmidt tolerance factor. Therefore, it was chosen an A

site and a B site (magnesium and tin) based on the computations for selenides made by Jess et al. (2022).

2.3.1 Preparation methods - Chemical Bath Deposition

There are several deposition techniques available today, but Chemical Bath Deposition (CBD), also known as solution growth, controlled precipitation, or simply chemical deposition, has emerged as one of the most used methods for the deposition of metal chalcogenide thin films. This approach is popular because it does not require complicated instrumentation such as a vacuum system or other costly equipment. [26] Deposition of metal chalcogenide thin films occurs in the CBD method when the substrate is kept in contact with a dilute chemical solution comprising metal and chalcogen ions. Those ions react and nucleation occurs on top of the substrate at low temperatures (<100 °C). [26]

The essential working principle of the CBD process is comparable to precipitation reactions and is dependent on the product's relative solubility. Precipitation happens when the concentration of the reactants exceeds the solubility of the product (K_{SP}) at a given temperature. When the contrary happens, the solid phase generated dissolves back into the solution. [27]

The solubility product of AB can be defined by equation (2.2), where $[A+]$ and $[B-]$ correspond to the concentration of the ions A and B, respectively, in the solution.

$$K_{sp} = [A+][B-] \tag{2.2}$$

Growth kinetics are influenced by the concentration of ions, their rate of deposition, and the processes of nucleation and growth on immersed substrates. Because the thermodynamics equilibrium can depend on the concentration of hydrogen ions, the pH of the reaction mixture influences thin film formation; a reduction in pH results in porous, non-reflective, powdery, and weakly adherent thin films on the substrates. This occurs because at higher pH, metal ion concentrations are lower, and the reaction rate is slower. [27]

Typically, a complexing agent is used in a bath to control the reaction, otherwise, spontaneous reaction and material sedimentation can occur. The complex's stability is also affected by the temperature and pH of the reaction bath.

In most cases, an increase in solution temperature makes the complex less stable, but an increase in pH makes it more stable. [27] Higher temperatures, in most situations, allow for increased grain formation, whereas lower temperatures result in very small nuclei in solution that are thermodynamically unstable. [26]

Normally, the chemical bath deposition process produces high-quality semiconductor thin films at a slow rate. The latter is important because powdery deposits and a lack of specular reflection are typically associated with higher deposition rates. [27] The composition of the chemical bath is crucial for the synthesis of high-quality thin films. The chemical and physical properties of the deposited thin film are influenced by the nature of the reactants. [27]

Even though it is extremely difficult to obtain a high-quality thin film after coating from a solution alone, it is possible to improve the quality and the properties of the films. [28] This, according to Kumar et al. 2022, can be achieved by performing thermal annealing in an inert atmosphere. Thermal annealing is a common technique for strengthening a solid by gradually raising, maintaining, and then lowering its temperature. Improvements of films can be seen after a post-deposition annealing treatment, which includes increasing crystallinity, tuning the crystal orientation, increasing grain size, diminishing porosity, and decreasing defect concentration. [28]

2.3.2 Characterization methods

Screening for new solar cell materials can be done by looking for band gaps in a suitable range within the perovskite family. [21] However, other methods can be used in order to fully characterize chalcogenide perovskites, such as X-ray diffraction pattern, UV-Vis spectrophotometry, photoluminescence intensity, X-ray photoelectron spectroscopy or Raman characterization. [7]

Electron microscopy, X-ray diffraction, and atomic force microscopy are common techniques used to improve, validate, and evaluate the quality of perovskite thin film fabrication methods. [30] Measurements in optoelectronics such as photoluminescence, electroluminescence, Raman, and UV-vis spectroscopy can assess carrier dynamics such as carrier generation, transport, and recombination. [30]

X-ray-assisted characterization techniques have proven to be effective tools for studying the crystal, electronic structure, and chemical composition of perovskite materials. They are frequently used to monitor the synthesis process because they can effectively distinguish the stages of crystallization development during annealing steps in perovskite film fabrication. [30]

The band gaps of a semiconductor can be calculated by application of the Tauc method. [15] This method assumes that α, the energy-dependent absorption coefficient can be expressed by the equation (2.3):

$$(\alpha \times hv)^{1/\gamma} = B \times (hv - E_g) \tag{2.3}$$

where h is the Plank constant, v is the frequency of the photons, E_g is the band gap energy, and B is a constant. The γ factor varies according to the type of electron transition and is equal to 0.5 or 2 for direct and indirect transition band gaps, respectively. Simply put, a direct band gap is present when an electron can directly emit a photon, whereas an indirect band gap is present when a photon cannot be emitted when the additional absorption as mission of a photon is required. [15]

3 Materials and Methods

3.1 Experimental procedures

The reagents used were sodium sulphite, 98+%, A. C. S. reagent, selenium powder, -100 MESH, 99.5+ %, sodium hydroxide solution C(NaOH)= 1 mol/l, tin (II) chloride dihydrate, 98%, magnesium chloride anhydrous, ≥98 %, triethanolamine (TEA), ethanolamine (ETA), ethylenediaminetetraacetic acid (EDTA), disodium salt dihydrate, 99 %, acetone, A.C.S. reagent, ≥99.5 %, ammonium hydroxide solution, A.C.S. reagent, 28.0-30.0 % NH_3 basis, nitric acid, A. C. S. reagent, 70 %, thiourea ≥99 % and selenium pellets, 1-6 mm.

Figure 3-1 - Set-up for the CBD.

To develop $MgSnSe_3$, first the deposition of tin selenide (SnSe) and magnesium selenide (MgSe) thin films were developed individually at ambient pressure on 2.5 x 2.5 cm^2 FTO or soda-lime glass (SLG).

The SLG glasses were cleaned using an ultrasonic cleaning process that included a detergent for ultrasonic and splash-cleaning in deionized water (DIW). The FTO were cleaned in a bath of ammonia, hydrogen peroxide, and water before being rinsed with deionized water. They were then immersed in acetone in an ultrasonic bath before being rinsed with isopropanol and DIW, following a previous cleaning protocol developed within the LaNaSC group.

The SnSe thin films were made based on the work of of Zainal et al. (2004). A fresh solution of sodium selenosulphate of 0.16 mol/L was prepared by mixing 15 g of sodium sulfite with 200 mL of DIW and 5 g of selenium powder. Later, it was constantly stirred on a hot plate in a 90 ºC water bath for ten hours. This solution was stirred and heated to 90 ºC before use and was not kept for more than four days.

In a 100 mL beaker, it was incorporated 2.62 g of tin chloride with 30 mL of DIW to make the chemical bath. 1 mol/L solution of NaOH was added with the goal of keeping the pH of the bath at 11.4 (≈ 24 mL). After that, 30 mL of the sodium selenosulphate solution was added. Back-to-back FTO or SLG were introduced vertically into the beaker using tweezers (Figure 3-1), and the optimum temperature and duration of the bath were studied. Throughout the process, the bath was left undisturbed. To make sure no liquid was evaporated, and the glasses were all at the same height in the bath, it was used aluminium foil.

Following a procedure described by Ubale et al. (2013), the MgSe thin films were formed in a 100 mL beaker containing 28 mL of 0.12 mol/L magnesium chloride, 14 mL of triethanolamine,

and 28 mL of a selenium dioxide (0.13 mol/L) solution. In the bath, the substrates were positioned vertically using tweezers. To make the selenium dioxide solution, 1 g of selenium powder was dissolved in nitric acid and boiled until a white residual powder was obtained. After that, the powder was dissolved in 100 mL of deionized water. The optimal temperature and duration of the bath were then investigated. [16]

An ultrasound machine was used to try to improve the uniformity of the thin films. Elma Schmidbauer Elmasonic P 60 H Ultrasonic Cleaning Unit was used for this.

Finally, to study the possibility of forming the desired chalcogenide perovskite, one species was deposed first, followed by the other species. Subsequently, the samples were thermally annealed to different temperatures for one hour (150 ºC, 250 ºC, 350 ºC, 450 ºC and 550 ºC). This thermal annealing occurred in a tube furnace (Figure 3-2) in the presence of two Se pellets next to the samples. Prior to the annealing, the tube was pumped and flushed with nitrogen three times, followed by two times with argon. A flow of argon of 100 sccm was used for the entire process and the heat ramp was 10 ºC/min.

Figure 3-2 - Tube furnace used for the annealing treatment.

To create an oxide perovskite, $MgSnO_3$, a deposition of MgSe and SnSe was performed on FTO glass. First, MgSe was deposited on top of SnSe, and then the reverse sequence was applied. The resulting samples were placed on a hot plate, heated to 500 ºC for a duration of 2-4 hours.

SnS thin films were synthesized by adding 1 g of tin chloride in a 150 mL beaker and dissolving it with 5 mL of acetone, with the help of a magnetic stirrer. Under continuous stirring it was added 5.5 mL of TEA to the previous solution. After getting a homogenous solution it was added 0.3 g of thiourea and was added 87.5 mL of DIW to the bath. The previously washed

glasses were put vertically with the assistance of tweezers in a beaker. This deposition was done at 70 °C for 1 h, following Chaki et al. 2016.

Babatunde et al. 2020 demonstrated a CBD method for producing MgS thin films. The process involved adding 20 mL of 1.0 mol/L magnesium chloride solution, followed by 20 mL of 1.0 mL thiourea solution and 20 mL of 1.0 mL of EDTA solution (instead of EDTA, TEA was also tested for the same concentration of EDTA). The bath was heated to 70 °C and had duration of 1 h.

3.2 Characterization

After the CBD, the samples were characterized using SEM, EDX, Raman spectroscopy, UV-Vis spectrophotometry, and XRD. The FEI Quanta 650 FEG SEM was used for SEM and EDX was done with INCAx-act. The WITec Alpha300R Confocal Raman Microscope was used for Raman spectroscopy. PANalytical's X'Pert PRO MRD was used for the XRD. The transmittance was measured with a Perkin Elmer Lambda 950 UV-VIS-NIR spectrophotometer equipped with integrating sphere technology.

The samples were characterized in SEM with top view to examine the surface topography and sample composition by EDX, while the thickness of the thin films was determined using a cross section setup. The compounds were identified using the Raman spectra. The band gap of the selected compounds was determined using UV-Vis Transmittance. The structure of the crystals in the sample was determined using XRD.

4 Results and discussion

Since chalcogenide photovoltaics is still in its early stages, it is important to improve the technology in terms of stability, performance, and process. [3] Because these compounds are usually fabricated under high temperatures, this project will investigate whether chalcogenide perovskites can be synthesized using the previously stated chemical bath deposition of two binary compounds, MgSe and SnSe. This work will also test various conditions in the CBD to optimize the process and produce better semiconductor films.

4.1 Fabrication of the thin films

For the fabrication of the materials, it was studied whether the deposition process advocated by Zainal et al. (2004) and Ubale et al. (2013) for SnSe and MgSe could be replicated. SLG was used in these experiments to determine whether deposition occurred.

Following Zainal et al. (2004) reports, it was observed a film growth after 1.5 h of deposition for a bath temperature of 45 ºC. The film-growth was more uniform after two hours of deposition. Figure 4-1 shows SEM images of the obtained SnSe thin films at 45 ºC with variation of time.

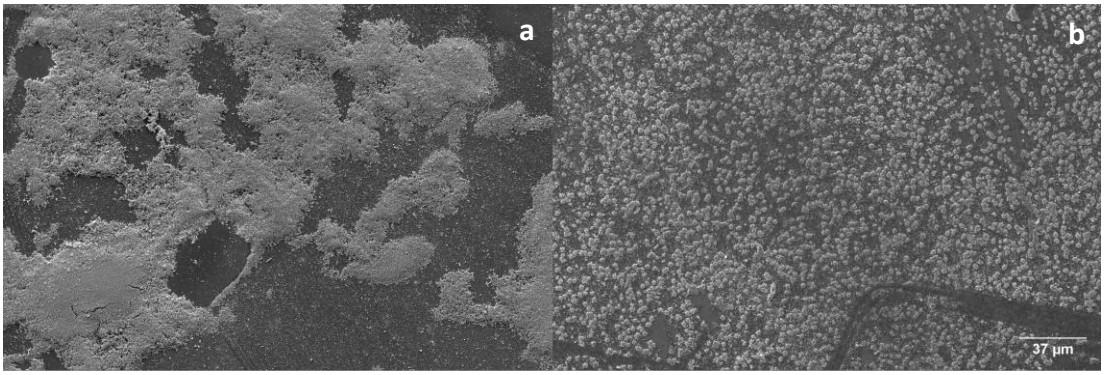

Figure 4-1 - SEM images for SnSe with bath temperature at 45 ºC and deposition time for 1.5 h (a) and 2 h (b).

Following the report of Ubale et al. (2013), it was investigated the deposition of the MgSe thin films for 6 h at room temperature. After this deposition time, by the naked eye it was hard to determine the existence of a film. Nevertheless, Figure 4-2 shows the SEM images where some crystals were obtained. In addition, EDX analysis revealed that magnesium selenide was present on the sample.

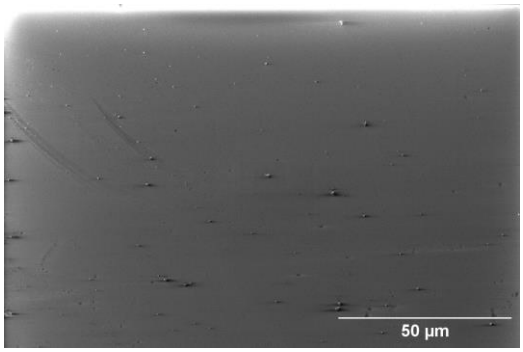

Figure 4-2 - SEM for MgSe CBD at room temperature for 6 h.

Because the deposition of crystals for the expected species was observed by SEM and EDX, the next step was to optimize the bath conditions.

4.2 Parameters that affect the thin films

In the first step, the optimization was focused on bath temperature and deposition time, and FTO was used as a substrate.

4.2.1 Temperature and deposition time

Since increasing the temperature in the bath may increase the quality of the films [26], the bath temperature for the deposition of tin selenide films was varied, with depositions done at 45 ºC, 70 ºC and 95 ºC. By naked eye it was possible to conclude that the increase in temperature corresponds with better deposition and a more homogenous thin film.

In addition to changing the temperature, the bath deposition time was studied within a range from 1.5 to 3 h. Figure 4-3 shows the SEM images for the different temperatures and deposition times.

Based on the results shown in Figure 4-3, a deposition duration of 2 h produced the most homogenous results across all temperatures (Figure 4-3b, 4-3e, 4-3h). Afterwards, it was determined that a bath temperature of 95 ºC resulted in the most uniform deposition (Figure 4-3h), and thus the bath with a deposition temperature of 95 ºC and a duration of 2 h was chosen as the best option.

After previously confirming that MgSe could be deposited at room temperature, an optimization process was conducted. This optimization was carried out by varying the temperature of the bath for 45 ºC, 70 ºC, and 95 ºC. Following that, the deposition time was studied for 1.5 h, 2 h and 3 h at the prior mentioned temperatures. The results obtained, that can be consulted in Figure 4-4, show a more uniform film when the deposition conditions

correspond to 95ºC for 2 h (Figure 4-4h).

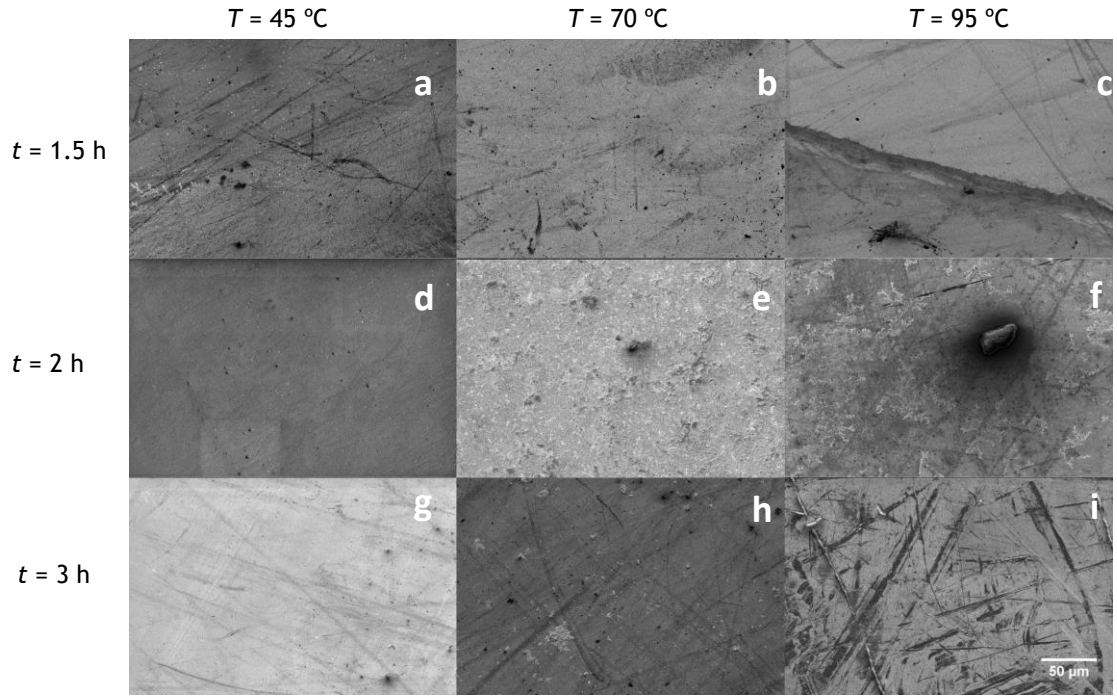

Figure 4-3 - SEM images of SnSe deposition for 45 ºC, 70 ºC and 95 ºC with deposition time of 1.5 h, 2 h and 3 h. The pictures have the following characteristics: a – 45 ºC, 1.5 h; b – 45 ºC, 2 h; c – 45 ºC, 3 h; d – 70 ºC, 1.5 h; e - 70 ºC, 2 h; f - 70 ºC, 3 h; g – 95 ºC, 1.5 h; h – 95 ºC, 2 h; i – 95 ºC, 3 h.

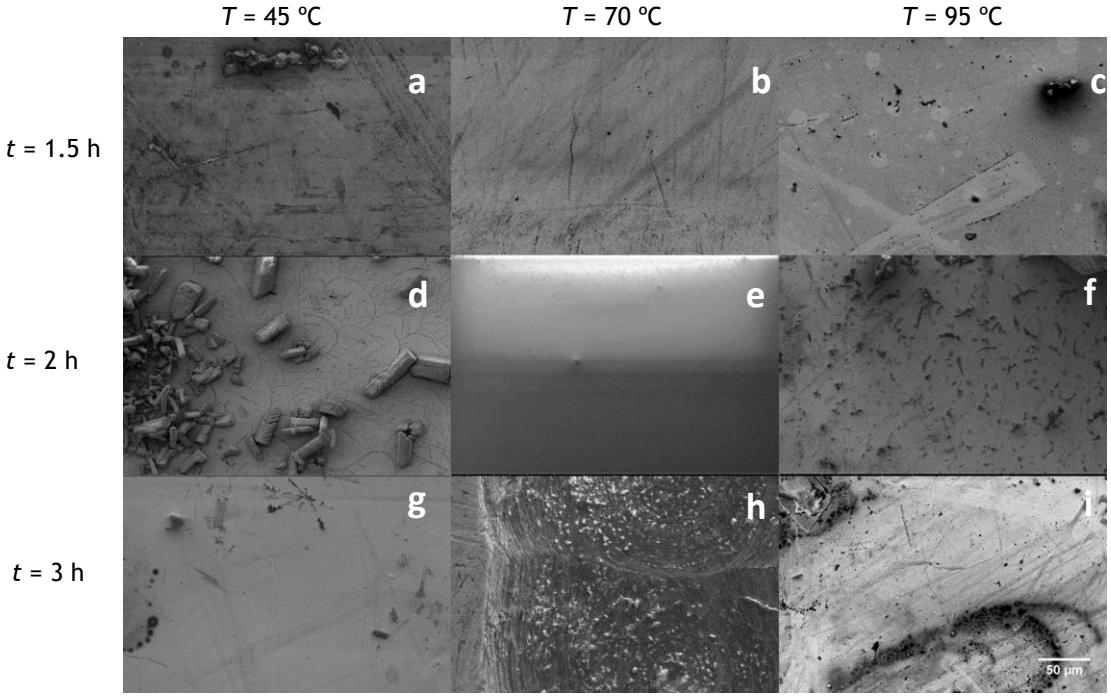

Figure 4-4 - SEM images of MgSe deposition for 45 ºC, 70 ºC and 95 ºC with deposition time of 1.5 h, 2 h and 3 h. The pictures have the following characteristics: a – 45 ºC, 1.5 h; b – 45 ºC, 2 h; c – 45 ºC, 3 h; d – 70 ºC, 1.5 h; e - 70 ºC, 2 h; f - 70 ºC, 3 h; g – 95 ºC, 1.5 h; h – 95 ºC, 2 h; i – 95 ºC, 3 h.

Unfortunately, the deposition of both SnSe and MgSe binary films did not result in very homogeneous films when viewed with SEM. Therefore, further optimization is required. In the future, the bath concentration should be changed and studied, the use of an ultrasound bath should be verified as well as see if a different complexing agent could be used. Since the baths are water based, a higher temperature cannot be achieved, due to the boiling point of water (100 ºC).

4.2.2 Ultrasound effect

Considering that the characteristics of the CBD bath are critical for deposition, it was investigated whether bath agitation had an impact. According to Salazar et al. (2006), agitating the baths can improve the quality of CBD thin films seeing as colloids and precipitates affect the film surface quality.

Hence, CBD for MgSe and SnSe was performed in an ultrasound bath at 80 ºC, which corresponds to the maximum temperature allowed by the equipment. This bath was performed at full equipment power and at 80 kHz, and the deposition time studied was 1 h and 2 h.

For both materials it could be seen deposition for these conditions, however the uniformity of the films was not improved. Through the results shown in Figure 4-5, it can be concluded that the films did not become more uniform. It is thought that the agitation of the ultrasound did not allow the crystals to deposit in the substrates.

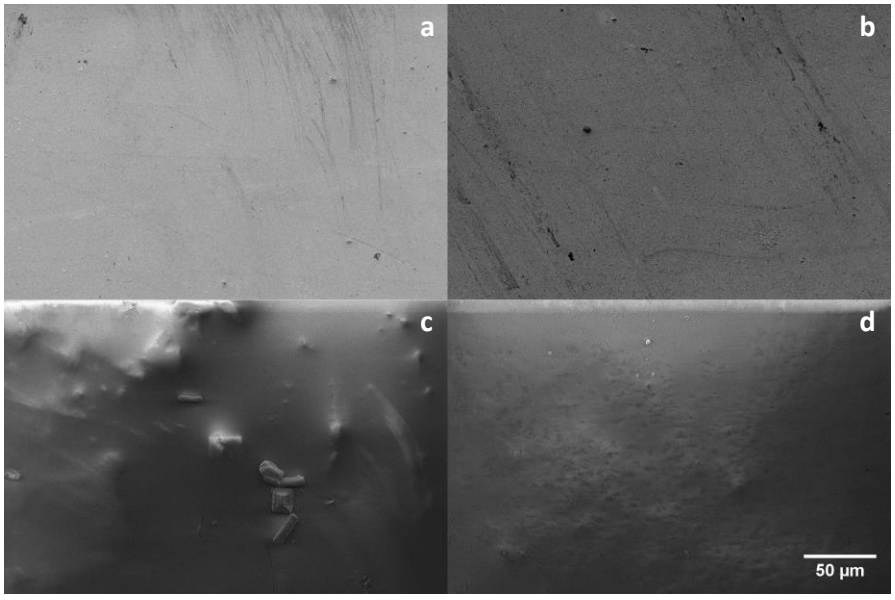

Figure 4-5 - SEM of the CBD samples for 80 ºC for 1 h and 2 h for MgSe and SnSe. This picture has as characteristics: a – SnSe, 80 ºC, 1 h; b – SnSe, 80 ºC, 2 h; c – MgSe, 80 ºC, 1 h; d – MgSe, 80 ºC, 2 h.

4.2.3 Complexing agent effect

LaNaSC group has previous knowledge in CBD, but those baths were done using ETA. Therefore, in the magnesium selenide bath it was exchanged the TEA for ETA to see its effect in the homogeneity of the thin films.

Figure 4-6 shows the SEM images for both complexing agents. Although deposition is visible by the naked eye with both reagents, when TEA is used (Figure 4-6a), there is more deposition, and it is more homogeneous.

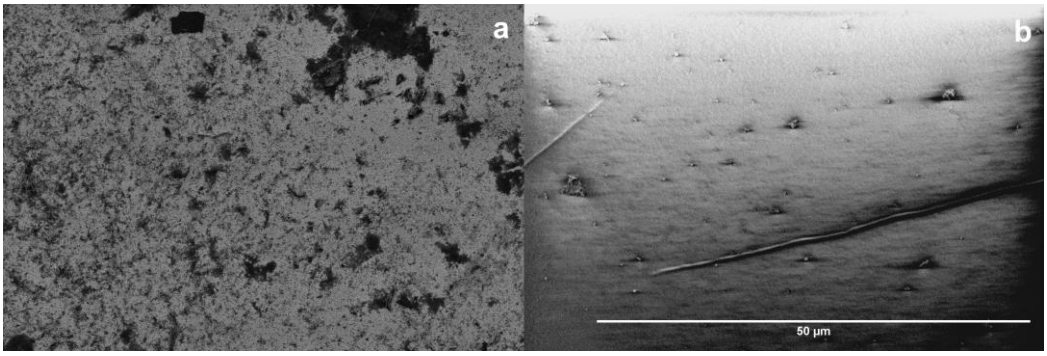

Figure 4-6 - SEM image for the MgSe thin film using TEA (a) and ETA (b) with deposition time of 2h at 95ºC.

4.2.4 Bath Concentration

As previously stated, the concentration of the precursors in a chemical bath deposition is critical because it affects the quality of the thin films positively or negatively. As a result, the effects of increasing or decreasing the concentration of the precursors in the baths were investigated.

The concentration of tin cations was studied from 0.32, 0.42 and 0.62 mol/L. For the magnesium cation it was from 0.09, 0.12 and 0.19 mol/L. Figure 10 shows the homogeneity of the different thin films obtained by modifying the concentration. In the case of SnSe, the concentration of 0.42 mol/L gave the best homogeneity (Figure 4-7b), while for MgSe a concentration of 0.12 mol/L resulted in more homogeneous films (Figure 4-7e). The best results were coherent with Zainal et al. (2004) and Ubale et al. (2013) conclusions.

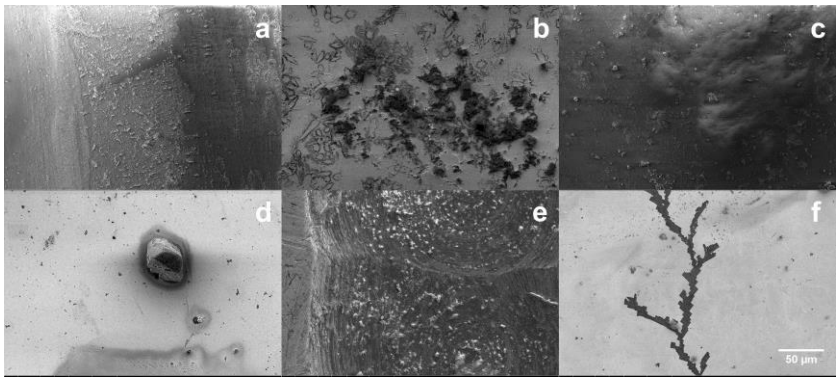

Figure 4-7 - SEM images for the different bath concentrations of the precursors. The characteristics are the following: a – SnSe, 0.32 mol/L; b – SnSe, 0.42 mol/L; c – SnSe, 0.62 mol/L; d – MgSe, 0.09 mol/L; e – MgSe, 0.12 mol/L; f – MgSe, 0.19 mol/L.

4.2.5 Structural study of SnSe and MgSe thin films

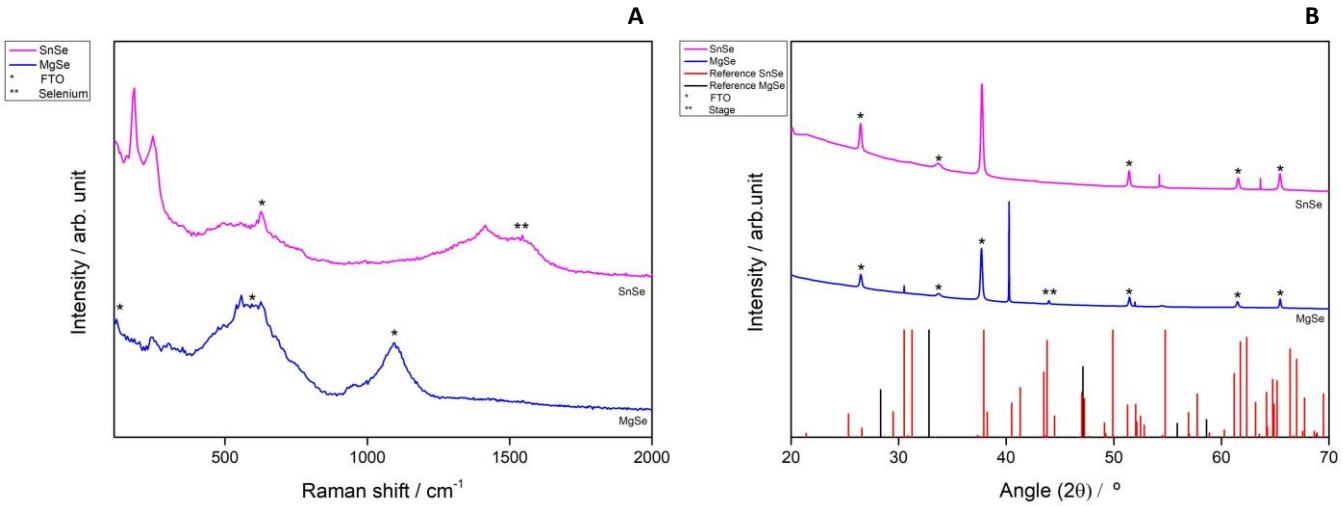

*Figure 4-8 - Raman spectrum (A) and XRD pattern (B) for MgSe (blue) and SnSe (pink) with deposition for 2 h at 95 ºC. The symbol * was used to represent the typical response of FTO glass, and ** to indicate the stage.*

The samples of MgSe and SnSe with deposition time of 2 h at 95 ºC were examined in Raman and XRD to see if the results corresponded with the literature. Figure 4-8A presents the Raman spectrum with the characteristic peaks for SnSe before 200 cm^{-1}. [17] Usually, MgSe presents a peak near 200 cm^{-1}, as it was stated by Rashad et al. (2020), however it is not possible to see it in Figure 4-8A. When analysing the XRD pattern, it is possible to see that for SnSe sample all peaks correspond to FTO or to the SnSe reference (the peaks are 38 º, 54.5 º and 63.6 º).

However, for the MgSe we can observe that the peaks correspond to FTO or Stage, and there are some peaks (for 30.5 º and 40.2 º) that do not correspond to the references and, thus,

were not identified. The stage is present in the reading and is a result of the machine analysis and of the small size of the sample used. To improve the comparability of the samples along the annealing experiments, thus not relying on different depositions, it was used a smaller size sample from the same deposition. The MgSe thin film had a thickness of 686.2 nm and SnSe thin film had 381.4 nm (see Appendix A for more information).

4.3 Production of the Perovskite

After the optimization process was concluded, for MgSe and SnSe individually, the creation of the chalcogenide perovskite was attempted. A hypothesis has been made after Nair et al. (2003) confirmed that it was possible to deposit two binary compounds via CBD, one on top of the other. Therefore, to form the chalcogenide perovskite, SnSe is going to be deposited on top of MgSe, and MgSe is going to be deposited on top of SnSe. Afterwards, a heat treatment will be conducted to form the perovskite.

4.3.1 Chalcogenide Perovskites with selenium

To create the desired perovskite by CBD, tin selenide was deposited in FTO, followed by the deposition of magnesium selenide, and the inverse was also studied. These depositions were carried out at 95 ºC for two hours.

After analysing in SEM images of both samples, as can be seen by Figure 4-9, it was possible to conclude that the films were more homogenous (in particular when MgSe was deposited on SnSe) when compared to the individual deposition of the binary compounds.

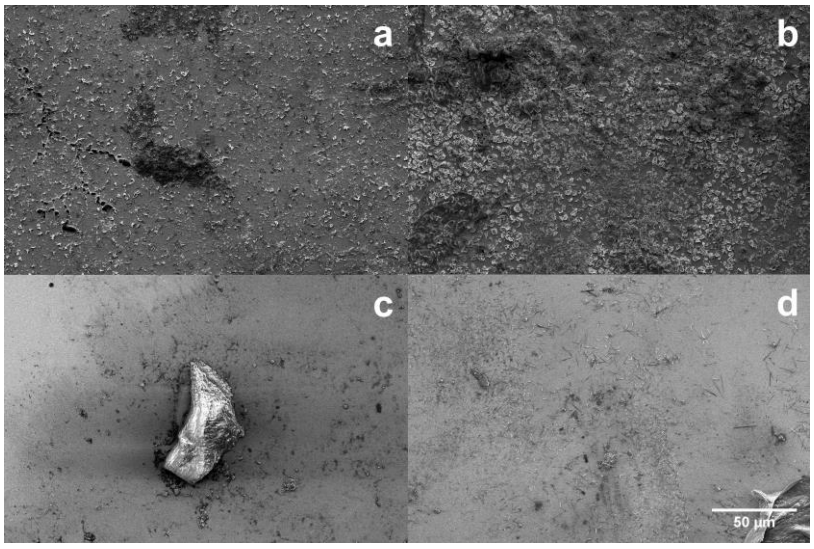

Figure 4-9 - SEM images of the as-deposited samples, where MgSe was deposited on SnSe (MgSe+SnSe, a and b) and SnSe was deposited on MgSe (SnSe+MgSe, c and d).

Figure 4-10 shows XRD patterns and Raman spectra of both samples as deposited. In the XRD patterns no peaks other than the ones of FTO or the stage were observed, indicating the deposition of amorphous thin films. In Raman spectra it is possible to see peaks corresponding to FTO, selenium (around 1500 cm^{-1}) and SnSe (typically around 200 cm^{-1}). The XRD pattern peaks for FTO and stage were previously studied, as well as the FTO peaks for Raman, and the results are present in Appendix B.

To study if a crystallization of the individual and studied thin films is achievable, thermal treatments were performed at 150 ºC, 250 ºC, 350 ºC, 450 ºC, and 550 ºC. It had previously been established that the samples used to produce the perovskites were amorphous.

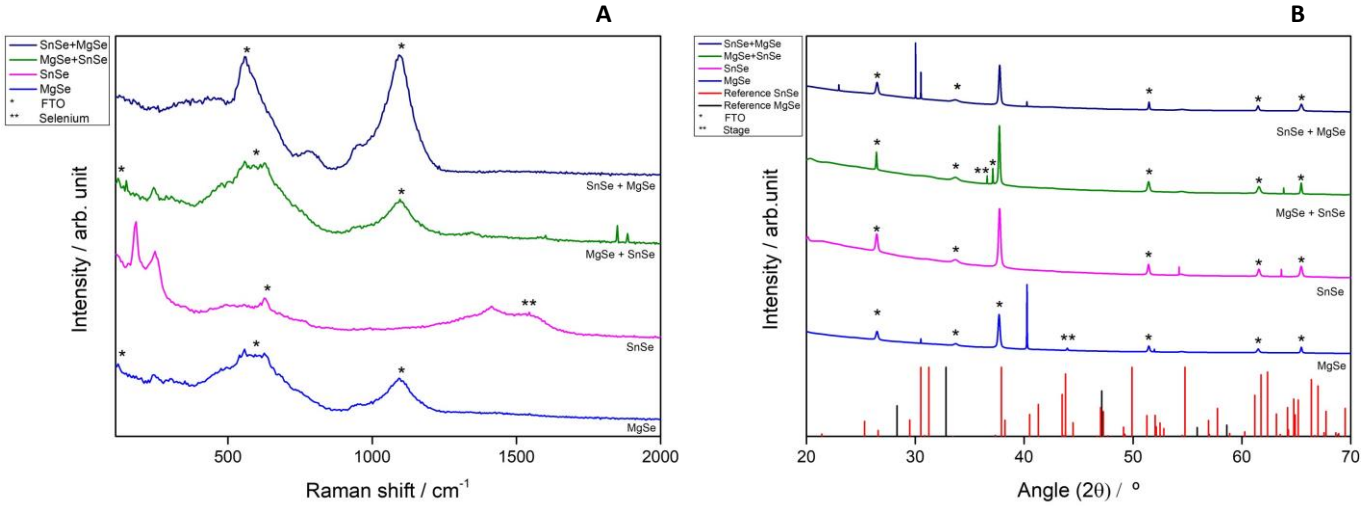

*Figure 4-10 - Raman spectrum (A) and XRD pattern (B) for the different compounds created for the perovskite as-deposited. The symbol * was used to represent the typical response of FTO glass, and ** to indicate the stage present in the reading.*

Based on the results of the analysis shown in Figure 4-11 and Figure 4-12, it can be concluded that no new peaks were discovered that were not caused by FTO or the reference materials MgSe and SnSe. [16] [17] Furthermore, because there has been no previous report of $MgSnSe_3$ formation, it is assumed that any new peaks observed may be indicative of the ABX_3 structure. As a result, based on the current data, it is not possible to conclude definitively that a perovskite material has been synthesized.

The heat treatment for the formation of the perovskite and improvement of the thin films was not performed at higher temperatures because it has been demonstrated that the perovskite material can suffer oxidation between 500 ºC and 600 ºC. [7] Nevertheless, there was not clear evidence of the formation of the oxygen perovskite. It has also been demonstrated that FTO coated glass cannot withstand temperatures above 700 ºC. [36]

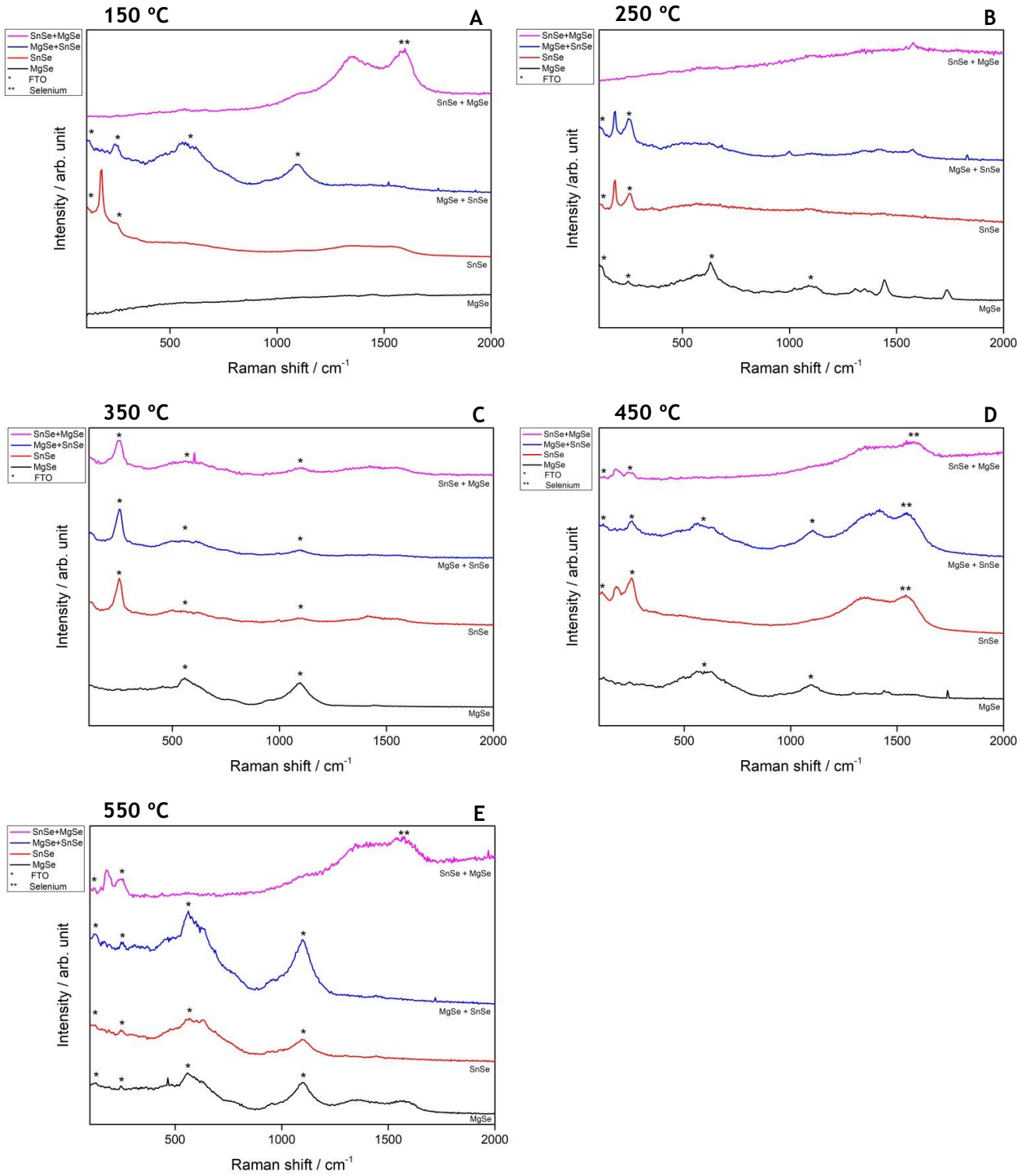

Figure 4-11 - Raman Spectra of the studied compounds for the annealing temperatures of 150 ºC (A), 250 ºC (B), 350 ºC (C), 450 ºC (D) and 550 ºC (E).

The materials could have also reacted with the oxygen present in the FTO, which could inhibit the formation of the selenide perovskite, since the annealing atmosphere in the tube furnace had only argon and selenium. This could be a possibility since the formation of oxide perovskites can be more stable than selenide perovskites. [8]

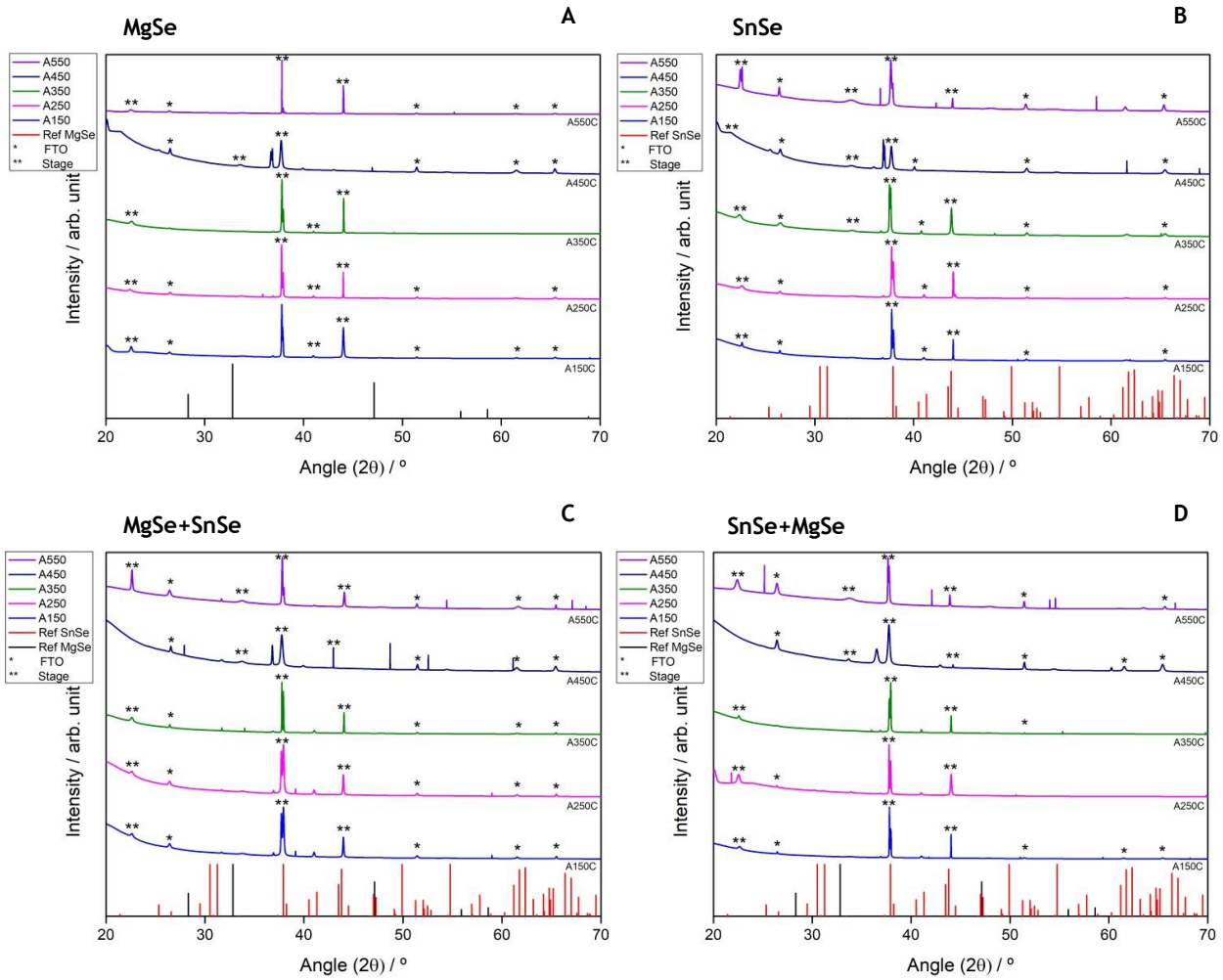

Figure 4-12 - XRD patterns for MgSe (A), SnSe (B), MgSe followed by SNSE deposition (C) and SnSe followed by MgSe deposition (D).

To determine whether a material is suitable for PV applications, its band gap must be determined. However, an accentuated drop characteristic of a good absorber was not observed in this study, which is required for the Tauc method. Regardless, Figure 4-13 and Figure 4-14 show the transmittance spectra for samples of MgSe, SnSe, MgSe on top of SnSe (MgSe+SnSe) and SnSe on top of MgSe (SnSe+MgSe) as deposited. Thus, the material absorbs in the expected range for perovskites (i.e., between 400 nm and 600 nm, as previously mentioned). In addition, the annealing process did not show any significant difference in the transmittance spectra, with a similar drop in the expected range. Here only the spectra corresponding to the samples annealed at 550 ºC is shown. The films presented a thickness between 292 – 3148 nm measured by SEM cross-section imaging (see appendix A for more information).

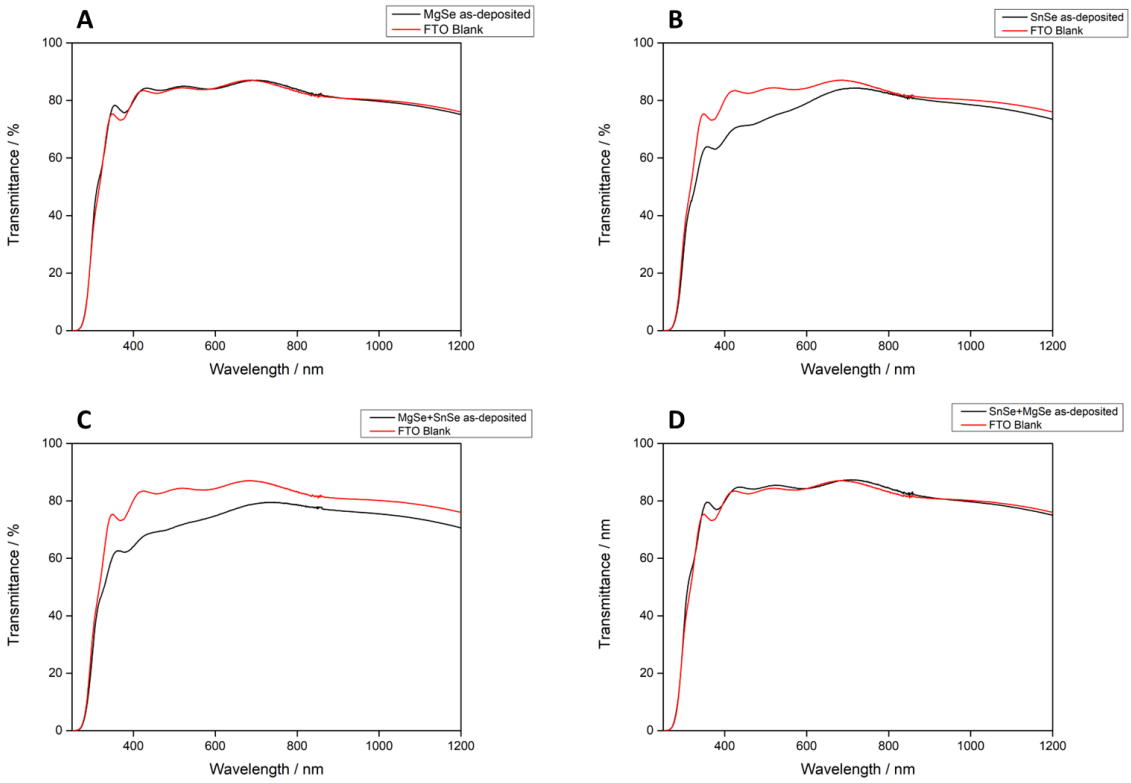

Figure 4-13 - Uv-Vis transmittance spectras for the MgSe (A), SnSe (B), MgSe+SnSe (C) and SnSe+MgSe (D) as-deposited.

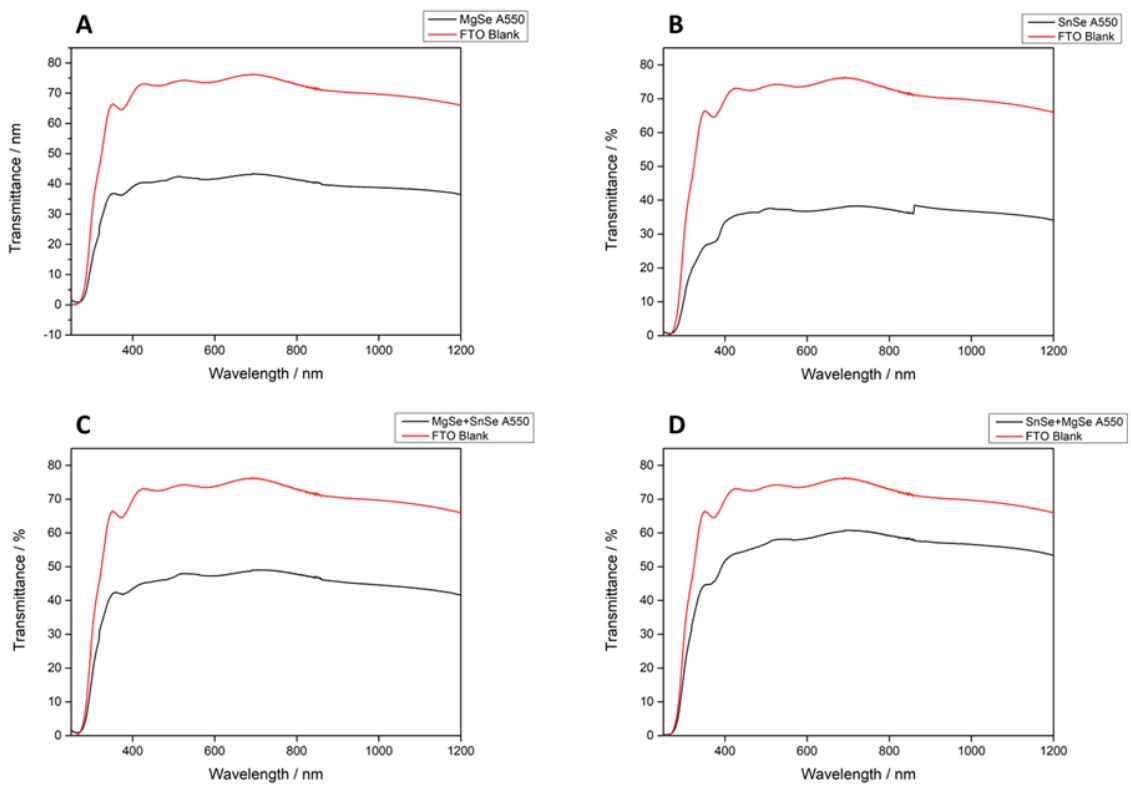

Figure 4-14 - Uv-Vis transmittance spectras for the MgSe (A), SnSe (B), MgSe+SnSe (C) and SnSe+MgSe (D) for an annealing treatment at 550 ºC.

4.3.2 Oxide Perovskite

To test the possibility of formation of the oxygen perovskite, another annealing setup was done. For this a deposited substrate was annealed on a hot plate in air atmosphere at 500 ºC. The obtained results in Figure 4-15 weren't consistent with those expected from the literature. [31] If $MgSeO_3$ was formed, there would be a peak at 38 º, which cannot be seen. The Raman spectra is not coherent with the formation of MgO_2 and does not show unexplained peaks. Therefore, it is not possible to conclude that an oxide perovskite was formed.

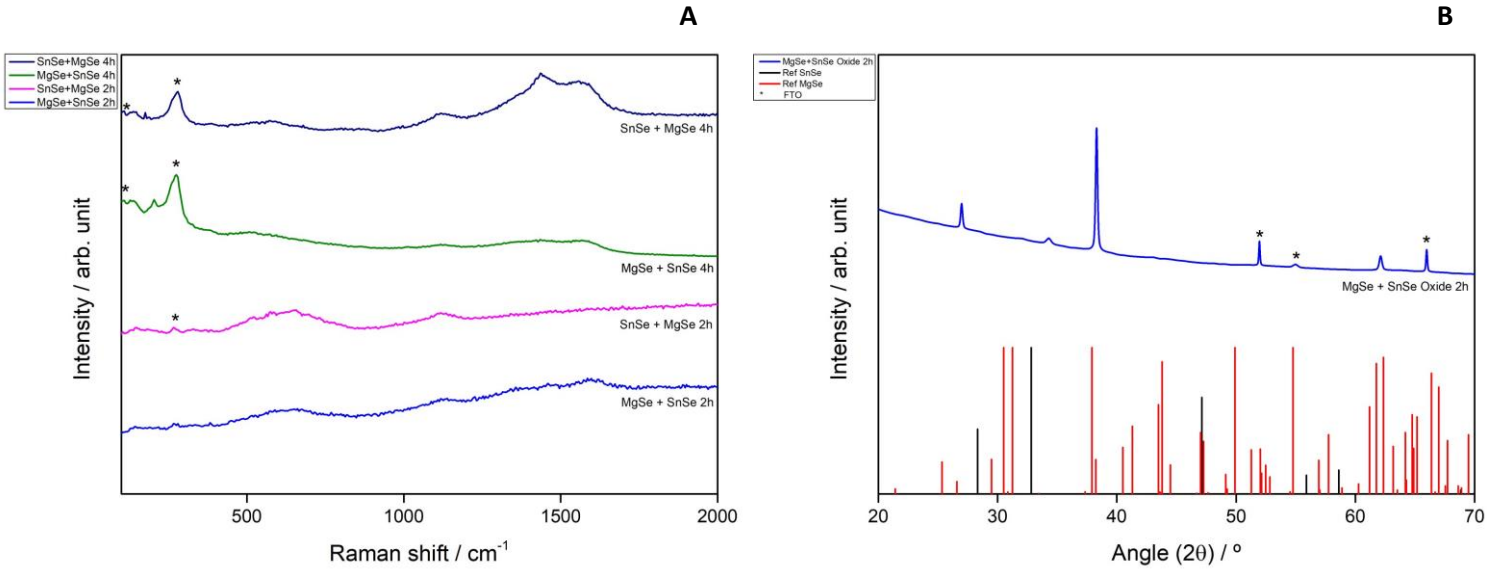

Figure 4-15 - XRD pattern (A) for the oxide perovskite with first deposited MgSe followed by SnSe, with annealing treatment duration of 2 h. Raman spectrum (B) for MgSe followed by SnSe depositions and vice-versa with thermal treatment for 2 h and 4 h.

4.3.3 Sulphide Perovskite

The selenide perovskites are significantly less stable than their sulphide counterparts, as expected given the decrease in octahedral and tolerance factors. [7] When comparing the sulphide radius with the selenides it is possible to see a reduction in terms of possible perovskite structure since larger anions must be balanced by larger cations. For sulphides, if the octahedral factor decreases for smaller B cations, then the probability of forming perovskites will decrease too. But this issue is worse for selenide compounds, since selenium has a smaller ionic radius than sulphur. [7] As a result, attempts were made to synthesize a sulphide perovskite using the same cations as before.

The deposition method initially stated used EDTA as a complexing agent. [32] However, as can be seen by Figure 4-16 the uniformity of the thin films using EDTA (Figure 4-16a) is worse than when using TEA (Figure 4-16b).

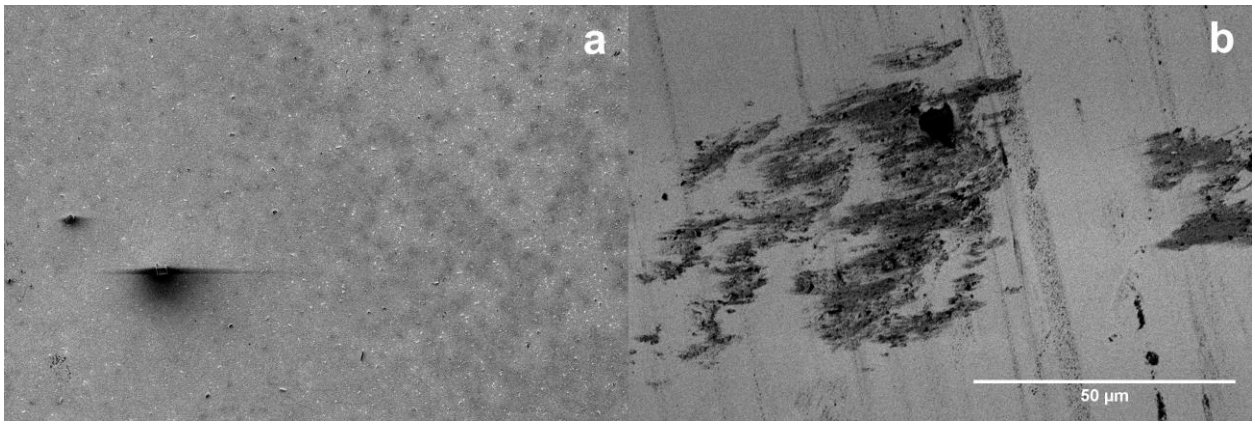

Figure 4-16 - SEM images for MgS deposited with EDTA (a) and TEA (b).

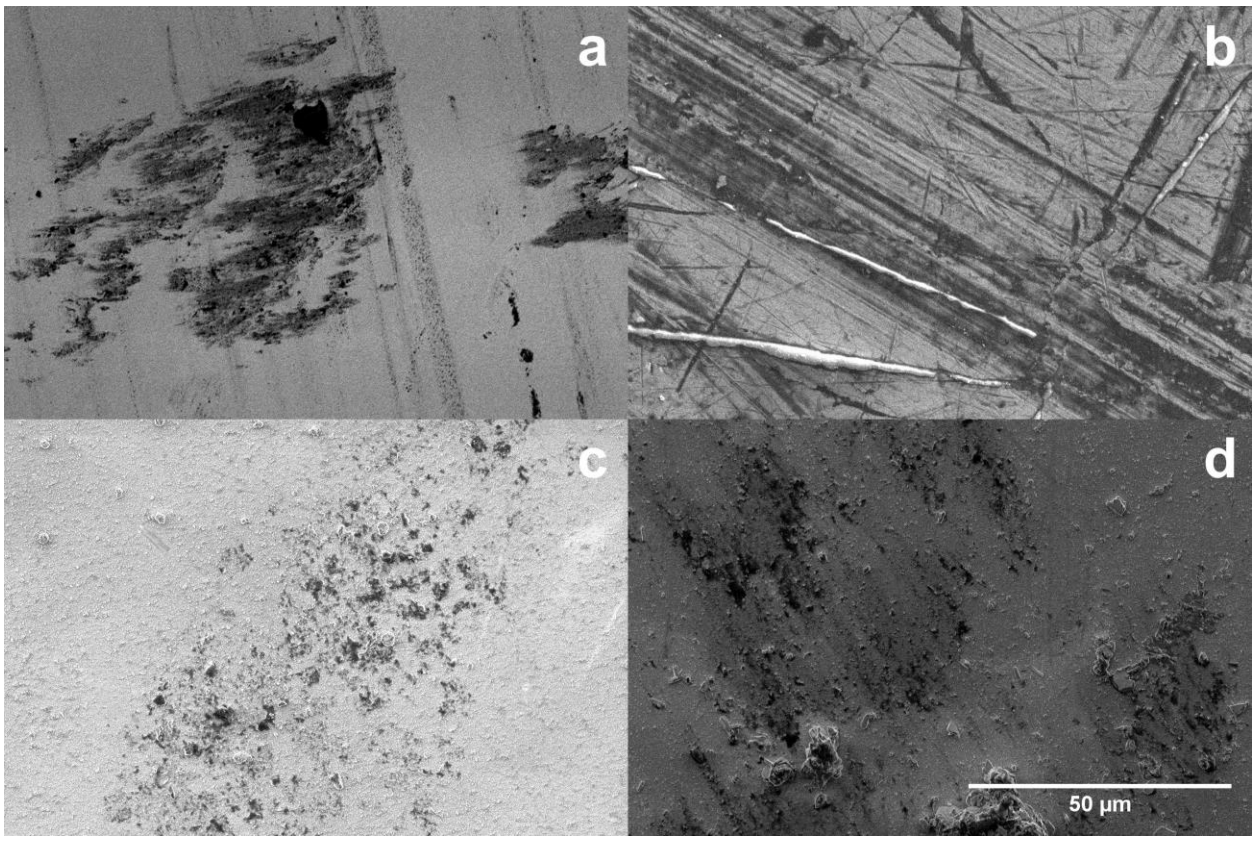

Figure 4-17 - SEM images for MgS (a), SnS (b), MgS deposited followed by SnS (c), and SnS deposited and MgS deposited after (d).

In Figure 4-17 it is possible to see that there was deposition, and after EDX analysis was carried out it could be confirmed that the deposited materials were the ones expected. According to the available literature, the spectra depicted in Figure 4-18 corresponds to the binary compounds MgS and SnS. [31] For MgS the Raman shift corresponds to 85, 205, and 285 cm^{-1}, whereas for SnS the Raman peaks should all be before 400 cm^{-1}. [31], [37] As a result, relying solely on Raman characterization to determine whether a sulphide perovskite has formed would be premature. Additional characterization is required to investigate whether the perovskite phase was formed. As previously stated, an annealing treatment could be beneficial to try to synthesize the sulphide perovskite.

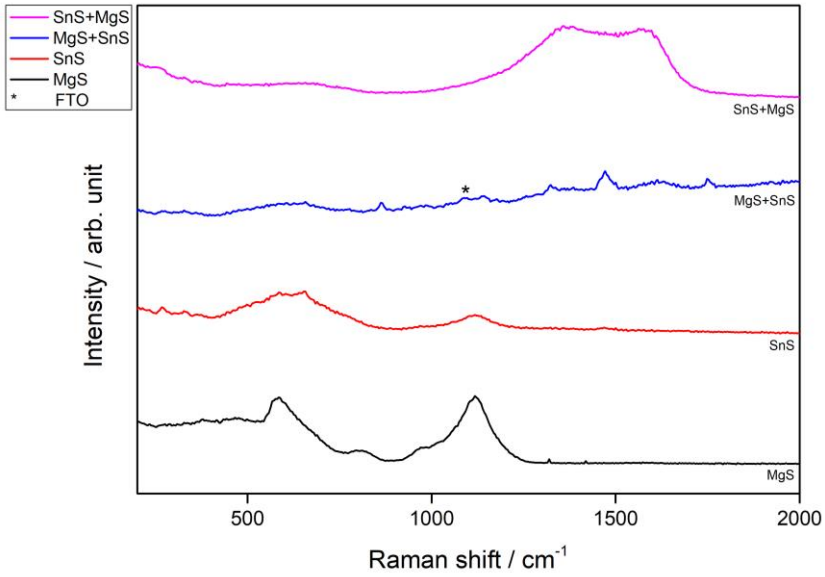

Figure 4-18 - Raman spectra for MgS, SnS, SnS deposited on top of MgS (MgS+SnS) and MgS deposited on top of SnS (SnS+MgS).

5 Conclusion

The main goal for this project was to synthesize $MgSnSe_3$ via chemical bath deposition. This method of deposition is low-cost and easily reproduceable, which makes it very interesting for possible industry reproduction.

Firstly, the binary salts of this compound (MgSe and SnSe) were deposited on FTO and after the confirmation of the deposition through EDX and SEM an optimization process was conducted. Through this optimization the thin films became more uniform. It was concluded that for MgSe the best complexing agent was TEA, and for MgSe and SnSe thin films the temperature of the bath should be 95 ºC with a duration of 2 h. Also, the ultrasound did not allow the deposition of crystals in the substrates.

Secondly, since the thin films deposited individually on the FTO, it was tried the sequential deposition of MgSe on top of SnSe and the deposition of SnSe on top of MgSe. The thin films showed more homogeneity when SnSe was deposited on top of MgSe. Afterwards, an annealing treatment was performed in an atmosphere of selenium and argon to see if the perovskite could be formed. This treatment went until 550 ºC and after characterization no positive results were seen.

Because the selenide perovskite could not be formed, an attempt to make an oxide perovskite was followed. The substrates of MgSe deposited on top of SnSe and of SnSe deposited on top of MgSe were heated on a hot plate on an air atmosphere at 500 ºC for 2h and 4 h. While analysing the characterization data it couldn't be confirmed the formation of this compound.

Since none of the perovskites above could be formed, a last attempt of synthesising a sulphide perovskite was made. It could be confirmed by SEM and EDX that MgS and SnS deposited on FTO. However, when the deposition at room temperature of MgS on top of SnS and the deposition of SnS on top of MgS was concluded, the data did not show the formation of a new compound.

Although the aim of the work was not achieved, this project succeeded in illuminating the LaNaSC group with respect to chalcogenide perovskites. Through this project it was possible to understand what isn't feasible in the creation of perovskite material and redirect future research.

6 Assessment of the work done

6.1 Objectives Achieved

The objective for this work was to create a chalcogenide perovskite ($MgSnSe_3$) via CBD using the binary compounds (MgSe and SnSe). While the deposition of the binary compounds was possible it needs more optimization to increase the uniformity of the thin films. The synthetization of the chalcogenide perovskite was not possible.

6.2 Other Work Carried Out

Since it was not possible to create the selenide perovskite, an attempt of creating and oxide and sulphide perovskite was carried out. It was not possible to make an oxide perovskite, nor a sulphide perovskite.

6.3 Final Assessment

During the development of this project, I became capable of doing characterization for SEM, EDX, Raman, and UV-Vis Transmittance on my own. I also had the opportunity to design the CBD processes. Since all the work necessary for this project was very hands-on, I had the opportunity to not only use all the knowledge obtained during my degree in photovoltaic technology but also further develop my knowledge in the solar cells area.

Due to the nature of this project, I had the ability to better learn about perovskite solar cells and chalcogenide perovskite solar cells. With this work, I could search for more sustainable ways of creating an absorber material for a solar cell.

7 References

[1] L. M. Goncalves, V. de Zea Bermudez, H. A. Ribeiro, and A. M. Mendes, "Dye-sensitized solar cells: A safe bet for the future," *Energy Environ Sci*, vol. 1, no. 6, pp. 655–667, 2008, doi: 10.1039/b807236a.

[2] Y. Y. Sun, M. L. Agiorgousis, P. Zhang, and S. Zhang, "Chalcogenide perovskites for photovoltaics," *Nano Lett*, vol. 15, no. 1, pp. 581–585, 2015, doi: 10.1021/nl504046x.

[3] J. George, A. P. Joseph, and M. Balachandran, "Perovskites: Emergence of highly efficient third-generation solar cells," *International Journal of Energy Research*. 2022. doi: 10.1002/er.8707.

[4] B. R. Sutherland, "Solar Materials Find Their Band Gap," *Joule*, vol. 4, no. 5. pp. 984–985, 2020. doi: 10.1016/j.joule.2020.05.001.

[5] Y. Y. Sun, M. L. Agiorgousis, P. Zhang, and S. Zhang, "Chalcogenide perovskites for photovoltaics," *Nano Lett*, vol. 15, no. 1, pp. 581–585, 2015, doi: 10.1021/nl504046x.

[6] S. A. Olaleru, J. K. Kirui, D. Wamwangi, K. T. Roro, and B. Mwakikunga, "Perovskite solar cells: The new epoch in photovoltaics," *Solar Energy*, vol. 196. pp. 295–309, 2020. doi: 10.1016/j.solener.2019.12.025.

[7] K. V. Sopiha, C. Comparotto, J. A. Márquez, and J. J. S. Scragg, "Chalcogenide Perovskites: Tantalizing Prospects, Challenging Materials," *Advanced Optical Materials*, vol. 10, no. 3. 2022. doi: 10.1002/adom.202101704.

[8] A. Jess, R. Yang, and C. J. Hages, "On the Phase Stability of Chalcogenide Perovskites," *Chemistry of Materials*, vol. 34, no. 15, pp. 6894–6901, 2022, doi: 10.1021/acs.chemmater.2c01289.

[9] S. P. Ratnayake, J. Ren, E. Colusso, M. Guglielmi, A. Martucci, and E. Della Gaspera, "SILAR Deposition of Metal Oxide Nanostructured Films," *Small*, vol. 17, no. 49. 2021. doi: 10.1002/smll.202101666.

[10] H. Soonmin, I. Paulraj, M. Kumar, R. K. Sonker, and P. Nandi, "Recent Developments on the Properties of Chalcogenide Thin Films." [Online]. Available: www.intechopen.com

[11] H. Soonmin, "Recent Advances in the Growth and Characterizations of SILAR-Deposited Thin Films," *Applied Sciences (Switzerland)*, vol. 12, no. 16, 2022, doi: 10.3390/app12168184.

[12] A. U. Ubale and Y. S. Sakhare, “Thickness dependent physical properties of chemically deposited nanocrystalline MgSe thin films deposited at room temperature by solution growth method,” *Mater Sci Semicond Process*, vol. 16, no. 6, pp. 1769–1774, 2013, doi: 10.1016/j.mssp.2013.06.015.

[13] F. G. Hone and T. Abza, “Short review of factors affecting chemical bath deposition method for metal chalcogenide thin films,” *International Journal of Thin Film Science and Technology*, vol. 8, no. 2. pp. 43–52, 2019. doi: 10.18576/ijtfst/080203.

[14] D. Tiwari, O. S. Hutter, and G. Longo, “Chalcogenide perovskites for photovoltaics: Current status and prospects,” *JPhys Energy*, vol. 3, no. 3, 2021, doi: 10.1088/2515-7655/abf41c.

[15] P. Makuła, M. Pacia, and W. Macyk, “How To Correctly Determine the Band Gap Energy of Modified Semiconductor Photocatalysts Based on UV-Vis Spectra,” *Journal of Physical Chemistry Letters*, vol. 9, no. 23. pp. 6814–6817, 2018. doi: 10.1021/acs.jpclett.8b02892.

[16] A. U. Ubale and Y. S. Sakhare, “Physical properties of MgSe thin films grown by chemical bath deposition method: Effect of molar concentration of MgCl2,” *Indian Journal of Physics*, vol. 87, no. 12, pp. 1183–1188, 2013, doi: 10.1007/s12648-013-0354-9.

[17] Z. Zainal, N. Saravanan, K. Anuar, M. Z. Hussein, and W. M. M. Yunus, “Chemical bath deposition of tin selenide thin films,” *Mater Sci Eng B Solid State Mater Adv Technol*, vol. 107, no. 2, pp. 181–185, 2004, doi: 10.1016/j.mseb.2003.11.008.

[18] N. Shahzad, N. Ali, I. Haq, S. Shah, S. Ali, Q. Ahmad, F. Azlullah, A. Kalam, A. Al-Sehemi, “Annealed tin selenide (SnSe) thin film material for solar cell application,” 2020.

[19] N. G. Park, “Perovskite solar cells: An emerging photovoltaic technology,” *Materials Today*, vol. 18, no. 2. pp. 65–72, 2015. doi: 10.1016/j.mattod.2014.07.007.

[20] B. G. Akinoglu, B. Tuncel, and V. Badescu, “Beyond 3rd generation solar cells and the full spectrum project. Recent advances and new emerging solar cells,” *Sustainable Energy Technologies and Assessments*, vol. 46, 2021, doi: 10.1016/j.seta.2021.101287.

[21] A. Swarnkar, W. J. Mir, R. Chakraborty, M. Jagadeeswararao, T. Sheikh, and A. Nag, “Are Chalcogenide Perovskites an Emerging Class of Semiconductors for Optoelectronic Properties and Solar Cell?,” *Chemistry of Materials*, vol. 31, no. 3. pp. 565–575, 2019. doi: 10.1021/acs.chemmater.8b04178.

[22] S. Perera, H. Hui, C. Zhao, H. Xue, F. Sun, C. Deng, N. Gross, C. Milleville, X. Xu, D. Watson, B. Weinstein, Y. Sun, S. Zhang, H. Zeng, "Chalcogenide perovskites - an emerging class of ionic semiconductors," *Nano Energy*, vol. 22, pp. 129–135, 2016, doi: 10.1016/j.nanoen.2016.02.020.

[23] S. Niu, J. Milam-Guerrero, Y. Zhou, K. Ye, B. Zhao, B. Melot, J. Ravichandran, "Thermal stability study of transition metal perovskite sulfides," *J Mater Res*, vol. 33, no. 24, pp. 4135–4143, 2018, doi: 10.1557/jmr.2018.419.

[24] S. Niu, H. Huyan, Y. Liu, M. Yeung, K. Ye, L. Blankemeier, T. Orvis, D. Sarkar, D. Singh, R. Kapadia, J. Ravichandran, "Bandgap Control via Structural and Chemical Tuning of Transition Metal Perovskite Chalcogenides," *Advanced Materials*, vol. 29, no. 9, 2017, doi: 10.1002/adma.201604733.

[25] J. S. Swinnea, H. Steinfink, L. E. Rendon-Diazmiron, and M. Gomezdaza, "The Crystal Structure of the 42-A Subcell of a Layer Structure with Approximate Composition Ba,Nb&," 1983.

[26] S. M. Pawar, B. S. Pawar, J. H. Kim, O. S. Joo, and C. D. Lokhande, "Recent status of chemical bath deposited metal chalcogenide and metal oxide thin films," *Current Applied Physics*, vol. 11, no. 2. pp. 117–161, 2011. doi: 10.1016/j.cap.2010.07.007.

[27] F. G. Hone and T. Abza, "Short review of factors affecting chemical bath deposition method for metal chalcogenide thin films," *International Journal of Thin Film Science and Technology*, vol. 8, no. 2. pp. 43–52, 2019. doi: 10.18576/ijtfst/080203.

[28] L. Sims, H. J. Egelhaaf, J. A. Hauch, F. R. Kogler, and R. Steim, "Plastic Solar Cells," *Comprehensive Renewable Energy*, vol. 1, pp. 439–480, 2012, doi: 10.1016/B978-0-08-087872-0.00120-7.

[29] M. Kumar, S. Rani, P. Vashishtha, G. Gupta, X. Wang, and V. N. Singh, "Exploring the optoelectronic properties of SnSe: a new insight," *J Mater Chem C Mater*, 2022, doi: 10.1039/d2tc03799h.

[30] M. cheol Kim, S. Y. Ham, D. Cheng, T. A. Wynn, H. S. Jung, and Y. S. Meng, "Advanced Characterization Techniques for Overcoming Challenges of Perovskite Solar Cell Materials," *Advanced Energy Materials*, vol. 11, no. 15. 2021. doi: 10.1002/aenm.202001753.

[31] S. H. Chaki, M. D. Chaudhary, and M. P. Deshpande, "SnS thin films deposited by chemical bath deposition, dip coating and SILAR techniques," *Journal of Semiconductors*, vol. 37, no. 5, 2016, doi: 10.1088/1674-4926/37/5/053001.

[32] R. A. Babatunde and Y. I. Bolanle, “Effect of Annealing on Optical and Electrical properties of Magnesium Sulphide (MgS) Thin Film Grown by Chemical Bath Deposition Method,” *Physics and Applied Sciences*, pp. 60–64, 2020, doi: 10.26438/ijsrpas/v8i3.6064.

[33] Y. A. Salazar, R. Patiño, J. L. Peña, W. Cauich, and A. I. Oliva, “Physical Properties of CdS/ITO Thin Films Growth by CBD Technique with Substrate Oscillating Agitation,” 2006.

[34] M. Rashad, S. D. A. Zaidi, and M. Asif, “Debating the magnesium–selenium battery technology,” *Journal of Magnesium and Alloys*, vol. 8, no. 4. pp. 980–988, 2020. doi: 10.1016/j.jma.2020.05.016.

[35] M. T. S. Nair, C. Lopéz-Mata, O. GomezDaza, and P. K. Nair, “Copper tin sulfide semiconductor thin films produced by heating SnS–CuS layers deposited from chemical bath,” *Semicond Sci Technol*, vol. 18, no. 8, pp. 755–759, 2003.

[36] J. K. Yang, B. Liang, M. J. Zhao, Y. Gao, F. C. Zhang, and H. L. Zhao, “Reference of Temperature and Time during tempering process for non-stoichiometric FTO films,” *Sci Rep*, vol. 5, 2015, doi: 10.1038/srep15001.

[37] C. Avril, V. Malavergne, R. Caracas, B. Zanda, B. Reynard, E. Charon, E. Bobocioiu, F. Brunet, S. Borensztanj, S. Pont, M. Tarrida, F. Guyot, “Raman spectroscopic properties and Raman identification of CaS-MgS-MnS-FeS-Cr2FeS4 sulfides in meteorites and reduced sulfur-rich systems,” *Meteorit Planet Sci*, vol. 48, no. 8, pp. 1415–1426, 2013, doi: 10.1111/maps.12145.

Appendice A – Thickness calculation

The thickness was calculated through cross section for the thin films of MgSe, SnSe, MgSe deposited on SnSe (MgSe+SnSe) and SnSe deposited on MgSe (SnSe+MgSe). After obtaining as least three measurements, the thickness was calculated with the help of the arithmetic average. These results can be seen in Table 1. The samples with A150 were annealed at 150 ºC, the samples with A250 suffered an annealing process of 250 ºC, the samples with A350 had a heat treatment of 350 ºC, the samples with A450 had a selenization of 450 ºC and the samples labeled with A550 had an annealing of 550 ºC. The samples with as deposited did not suffer a heat treatment, the were analyzed after the CBD of 95 ºC for 2 h.

Table 1 - Thickness for the selenide perovskites.

Sample (FTO)							Units	Average
MgSe as deposited	659.9	614.6	708.6	620	760.1	754.2	nm	686.2
SnSe as deposited	226.8	197.2	434	503	315.7	611.8	nm	381.4
MgSe+SnSe as deposited	586.6	394	409.7	906.8	651	712.5	nm	610.1
SnSe+MgSe as deposited	486.9	581.7	189.8	242.4	446.5	2.97.5	nm	389.5
MgSe A150	188	242.1	201.9	231.3	660.7	347.3	nm	311.9
SnSe A150	2.67	2.89	2.89	4.22	4.44	1.78	µm	3.1
MgSe+SnSe A150	838.6	537.8	648.4	570.1	806	484	nm	647.5
SnSe+MgSe A150	1.33	1.39	0.38	0.38	0.76	0.76	µm	0.8
MgSe A250	484	806	403	1610	-	-	nm	825.8
SnSe A250	1049	1097	1287	224.9	271.9	319.2	nm	708.2
MgSe+SnSe A250	1299	330.2	418.5	418.5	440.9	-	nm	581.4
SnSe+MgSe A250	424.9	865.7	904.2	943.2	442.8	-	nm	716.2
MgSe A350	-	-	-	2.02	0.7646	0.8986	µm	1.2
SnSe A350	551.4	800.7	893.7	862.7	381.9	549.2	nm	673.3
MgSe+SnSe A350	482.9	451.9	983.6	13.3	-	-	nm	482.9
SnSe+MgSe A350	406.7	281.6	283.3	251.4	553	605.4	nm	396.9
MgSe A 450	609.8	942.9	609.8	527.4	416.8	776.1	nm	647.1
SnSe A450	598.4	872.5	461.4	885.3	393.6	687.9	nm	649.9
MgSe+SnSe A450	794.9	905	877.2	603	740.6	548.2	nm	744.8
SnSe+MgSe A450	493.9	559.7	659.3	625.6	889.6	-	nm	645.6
Mg A550	149.5	135.5	128.3	156.6	235	192.3	nm	166.2
SnSe A550	312.5	341.2	454.8	369.3	539.8	639.9	nm	442.9
MgSe+SnSe A550	576.3	494.2	687.5	849.7	357.4	658.4	nm	603.9
SnSe+MgSe A550	435.9	410.3	283.2	181.3	236.4	205.1	nm	292

Appendice B – FTO values for XRD pattern and Raman spectrum and Stage values for XRD pattern

To make the characterization of the samples reliable it is necessary to obtain the peaks of the Raman spectrum and the XRD pattern for the FTO. It is also important to obtain the Stage peaks. These results can be analyzed in Figure A-1.

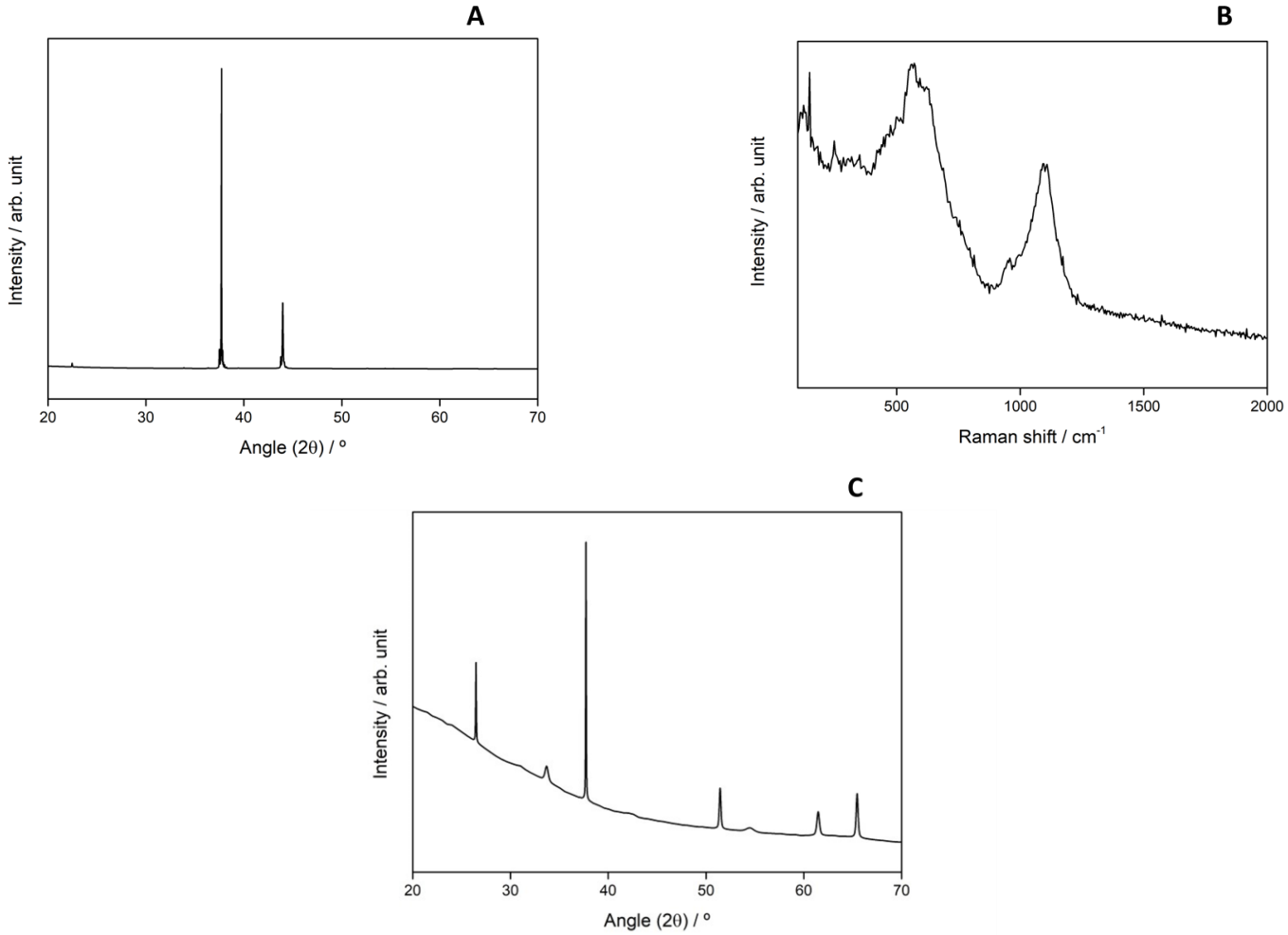

Figure A-7-1 – XRD pattern for the Stage (A), Raman spectrum for the FTO (B) and XRD pattern for the FTO (C).